Angewandte
Eine Zeitschrift der Gesellschaft Deutscher Chemiker
Chemie

Supporting Information

Palladium-Catalyzed Directed *meta*-Selective C–H Allylation of Arenes: Unactivated Internal Olefins as Allyl Surrogates

Tapas Kumar Achar[+], *Xinglong Zhang*[+], *Rahul Mondal, M. S. Shanavas, Siddhartha Maiti, Sabyasachi Maity, Nityananda Pal, Robert S. Paton,* and Debabrata Maiti**

anie_201904608_sm_miscellaneous_information.pdf

Supporting Information

69451 Weinheim, Germany

Palladium-Catalyzed Directed *meta*-Selective C–H Allylation of Arenes: Unactivated Internal Olefins as Allyl Surrogates

Tapas Kumar Achar,[a],† Xinglong Zhang,[b],† Rahul Mondal,[a] Shanavas M. S.,[a] Siddhartha Maiti,[c] Sabyasachi Maity,[a] Nityananda Pal,[a] Robert S. Paton, *[b] and Debabrata Maiti*[a]

[a]Department of Chemistry, Indian Institute of Technology Bombay, Powai, Mumbai 400076, India

[b]Chemistry Research Laboratory, University of Oxford, Mansfield Road, Oxford OX1 3TA, United Kingdom

[c]BSBE, Indian Institute of Technology Bombay, Powai, Mumbai 400076, India

† These authors contributed equally.

* Debabrata Maiti: dmaiti@chem.iitb.ac.in

* Robert S. Paton: robert.paton@colostate.edu

Abstract: Palladium(II)-catalyzed *meta*-selective C–H allylation of arenes has been developed utilizing synthetically inert unactivated acyclic internal olefins as allylic surrogates. The strong σ-donating and π-accepting ability of pyrimidine-based directing group facilitates the olefin insertion by overcoming inertness of the typical unactivated internal olefins. Exclusive allyl over styrenyl product selectivity as well as *E*-stereoselectivity were achieved with broad substrate scope, wide functional group tolerance and good to excellent yields. Late-stage functionalisations of pharmaceuticals were demonstrated. Experimental and computational studies shed insights on the mechanism and pointed to key palladacyclic steric control in determining product selectivities.

2.9. Computational Methods

Density functional theory (DFT) calculations were performed with *Gaussian 16* rev. A.03.[1] Geometry optimisations were carried out using recently developed global-hybrid meta-NGA (nonseparable gradient approximation) MN15 functional[2] with a mixed Karlsruhe-family basis set of triple-ζ valence def2-TZVPPD (where 'D' indicates diffuse basis functions) for Pd[3] atom and def2-SVP[4,5] for all other atoms (BS1). This functional was chosen as it performs much better than many other functionals in predicting transition metal reaction barrier heights.[2] Previously, Pd(II)-catalysed C-C bond formations have been studied using other functionals including meta-GGA TPSS and range-separated ωB97X-D functionals.[6,7] MN15 has been shown to give better agreement in geometry predictions of both transition metal complex and organic molecules than many other functionals including ωB97X-D and TPSS.[2] Minima and transition structures on the potential energy surface (PES) were confirmed as such by harmonic frequency analysis, showing respectively zero and one imaginary frequency, at the same level of theory. Single point (SP) corrections were performed separately with either MN15 or ωB97X-D[8] functional and def2-QZVPP[4] basis set for all atoms. The SMD continuum solvation model[9] was carried out to include the effect of acetonitrile solvent on the computed Gibbs energy profile. Gibbs energies were evaluated at 363.15 K, using a quasi-RRHO treatment of vibrational entropies.[10,11] Vibrational entropies of frequencies below 100 cm^{-1} were obtained according to a free rotor description, using a smooth damping function to interpolate between the two limiting descriptions. The free energies were further corrected using standard concentration of 1 mol/L, which were used in solvation calculations. SMD(acetonitrile)-ωB97X-D/def2-QZVPP//MN15/BS1 Gibbs energies were given with SMD(acetonitrile)-MN15/def2-QZVPP//MN15/BS1 Gibbs energies given in brackets throughout. All values are quoted in kcal mol^{-1}.

The *.wfn* files for NCIPLOT were generated at MN15/DGDZVP[14,15] level of theory. Noncovalent interaction (NCI) indices calculated with NCIPLOT were visualised at gradient isosurface value of $s = 0.5$ au. These are coloured according to the sign of (λ_2) over the range of –0.1 (blue = attractive) to +0.1 (red = repulsive). All molecular structures and molecular orbitals were visualized using *PyMOL* software.[16] Dihedral scans were done in gas phase using MN15/def2-SVP and the energies were taken without further corrections.

Geometries of all optimized structures (in *.xyz* format with their associated energy in Hartrees) are included in a separate folder named *structures_xyz* with an associated README file. All these data have been deposited with this Supporting Information and uploaded to zenodo.org (DOI: 10.5281/zenodo.2775841).

All Python scripts used for data analysis have been made available - https://github.com/bobbypaton - under a creative commons CC-BY license.

2.9.1 Conformational considerations for starting materials

The starting materials for computational modelling, sulfonyl arene, **1a**, and *trans*-hex-3-ene, were first conformationally sampled. The possible rotamers for sulfonyl arene, **1a**, were generated by systematically varying a combination of key dihedral angles shown in red (Scheme S1) and optimising the structures. The crystal structure of *trans*-hex-3-ene was obtained as a starting point for structure optimisation; additional rotamers were generated by varying the given dihedral angle in red (Scheme S1) and doing structural optimisations. The lowest energy conformers for each starting material were used for subsequent calculations.

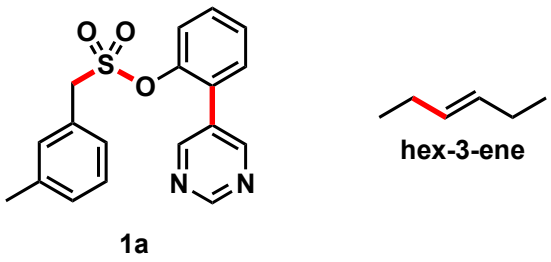

Scheme S1. Rotamers were generated by varying the dihedral angles in red in conformational sampling of the most stable conformer used for reaction modelling.

2.9.2 C–H activation in the presence of ligand

The amino acid ligand, *N*-Ac-norleucine, lowered the C–H activation barrier by forming a 5-membered palladacyle as shown in the main text (**ts-1'** at 20.0‡ (20.8‡) kcal mol^{-1}). Other possible arrangements of this ligand were found to have higher activation barriers than **ts-1'** (Figure S13).

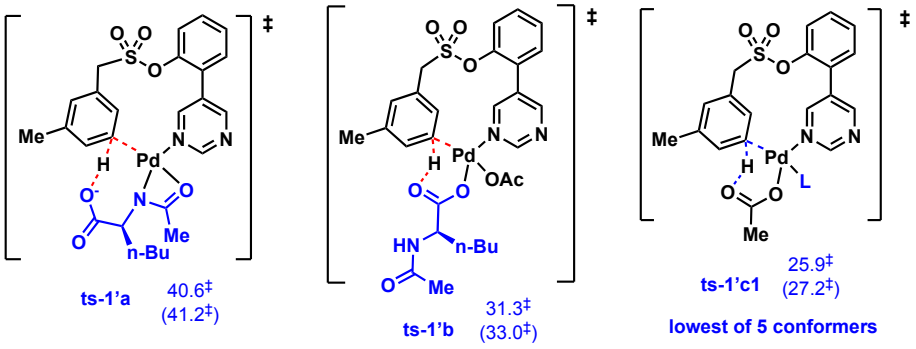

Figure S13. Possible arrangements of ligand for C–H activation step. Gibbs energies are given in kcal mol^{-1}.

2.9.3 Exact identity of the ligand in 1,2-migratory insertion TDTS

The intermediate after MPAA ligand-assisted C–H activation (**int-2'**) has the resulting ligand in imidic acid form. The subsequent 1,2-migratory insertion TS leading from here (**ts-3'a** at 41.7 kcal mol^{-1}, Figure S14) has a much higher barrier than its tautomeric form (**ts-3'b** at 27.1 kcal mol^{-1}, Figure S14). The coordination by acetate (**ts-3** at 23.2 kcal mol^{-1}, Figure S14) has the lowest barrier amongst these three possibilities. We anticipated that **ts-3** and **ts-3'b** would be rather close in energy, since they both coordinate to Pd-centre in a monodentate fashion (Figure S14), where the Pd–N interactions would dominate over other possible non-covalent interactions (NCIs) in the side chains. Although the amino acid side chain could provide better NCIs than the methyl group in acetate, it could also give rise to potentially more steric hinderance.

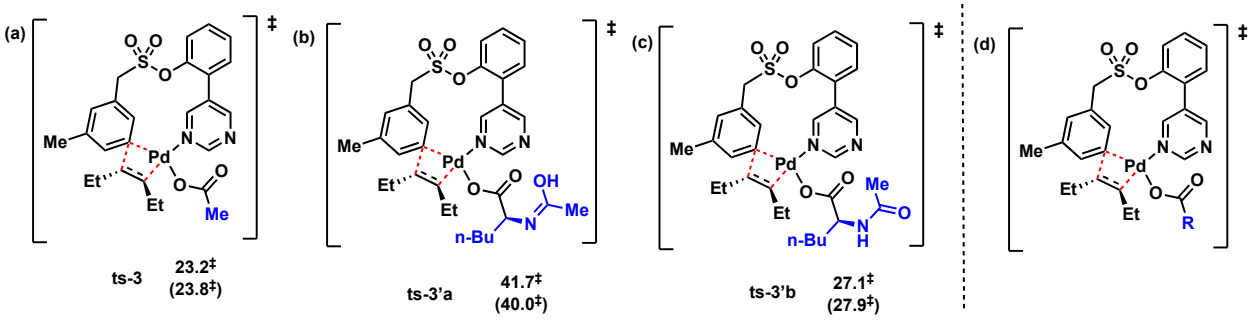

Figure S14. TDTSs with either acetate (a) or amino acid in tautomeric forms (b and c) as the monodentate ligand. These can be thought of having the structure in (d) where the R-groups vary. Gibbs energies are given in kcal mol^{-1}.

In the computational study of similar systems where amino acid ligands were used for the C–H activation step, the amino acid (a.a.) was retained as a monodentate ligand for all subsequent steps.[17,18] We envisioned that the acetate ligand and the a.a. ligand would have similar effects in 1,2-migratory insertion step and replacing the a.a. ligand with acetate would not affect the energy profile too much (Note that the main role of the a.a. ligand is in the C–H activation step). Conformational searches were thus performed for the 1,2-migratory insertion step above with either acetate or amino acid as the monodentate coordinating ligand. A total of 6 TSs were found for acetate ligand and 11 TSs for the a.a. ligand (these structures are given in folder *3_ligand_identity_in_TDTS* accompanying this ESI). All these are higher than C–H activation barrier, as expected since this step was overall rate-determining and C–H activation is reversible as measured by kinetic isotopic effect experimentally. Although the lowest barrier TSs were those with the a.a. ligand, these are really close in barrier to those of the lowest TS with acetate ligand (within 2 kcal mol^{-1}). For modelling purposes, it is sufficient to use acetate instead of the full a.a. ligand since the conclusion of the mechanism will remain the same.

2.9.4 Relative stabilities of int-5 and int-7 and β-hydride elimination TSs

We found, via intrinsic reaction coordinates (IRC) analyses, that **int-5** eventually lead to the product formation via direct β-hydride elimination (**ts-5**, Figure 5 main text) forming a metal-bonded Pd(II) hydride, whereas **int-7** underwent acetate-assisted β-hydride elimination (**ts-7**) with much lower activation barrier. **Int-7** was much more stable than **int-5** since in the latter, the acetate group was near the 14-membered palladacycle ring, giving rise to unfavourable interactions with the arene, as shown in the NCI plot (circled in green) in Figure S15. Alternative TSs for β-hydride elimination following each of these intermediates were given in Figure S16. Note that **ts-7'**, having the Pd-coordinating acetate-O atom forming 3-membered ring in the TS is much less favoured than **ts-7**, which has the non-coordinating acetate-O atom forming 5-membered ring.

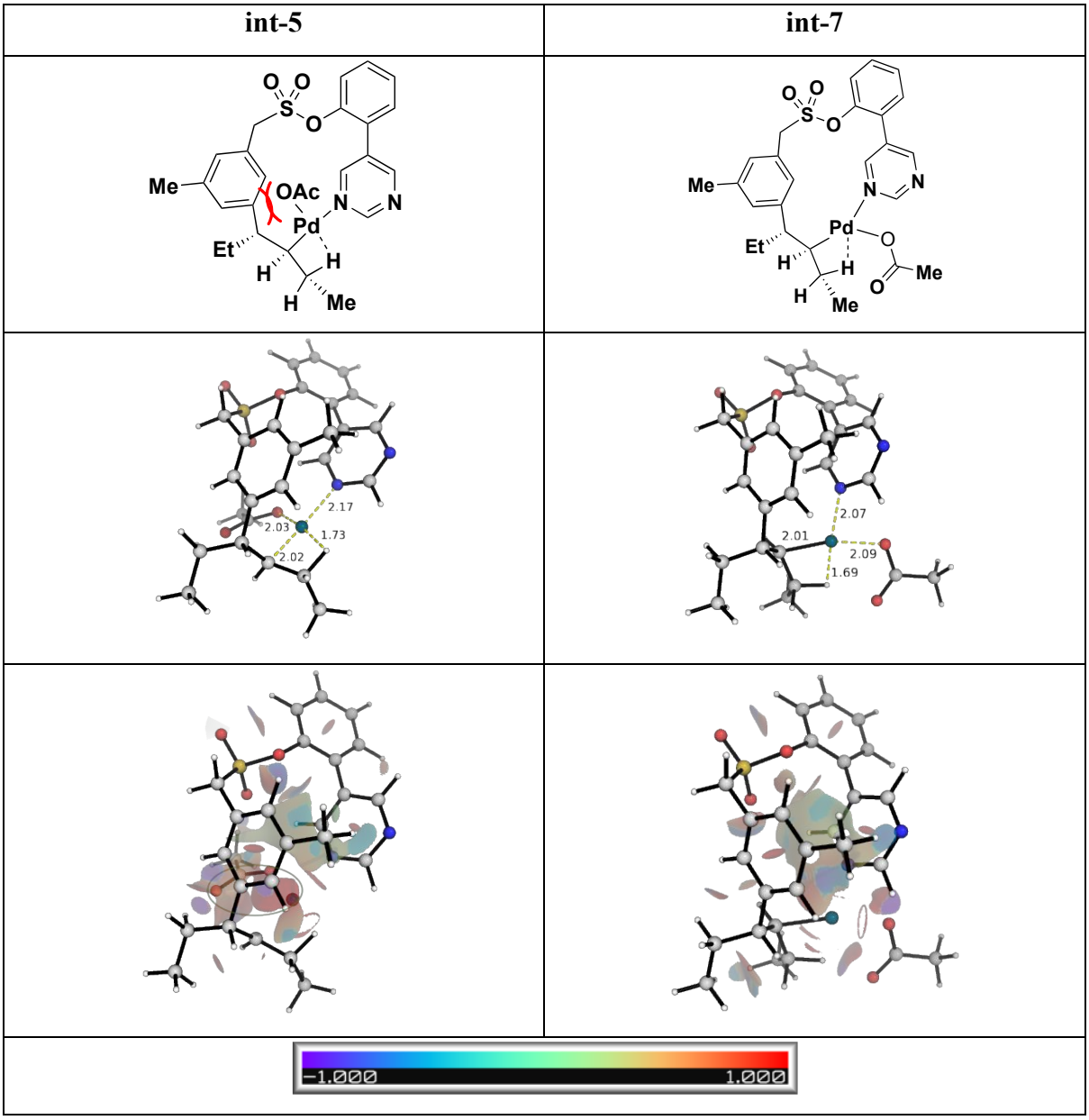

Figure S15. Relative stabilities of **int-5** and **int-7** and their NCI plots to indicate the sterics present.

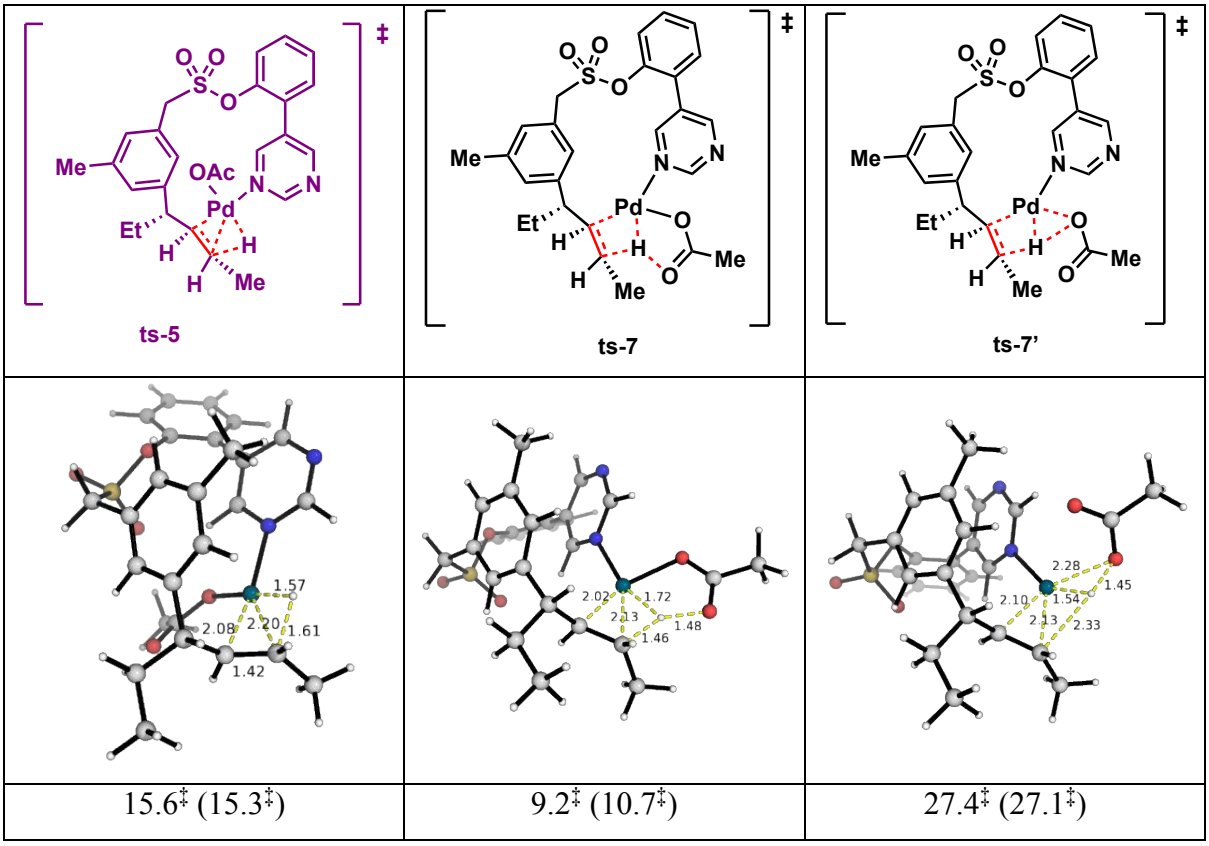

Figure S16. Alternative TSs for *β*-hydride elimination step to form the final product.

2.9.5 Product selectivity studies for *trans*-hexene substrate

The formations of both *E*- and *Z*-allylated products proceed via ligand-assisted *β*-hydride elimination whereas styrenylation proceeds via direct *β*-hydride elimination due to unfavourable arrangement of the acetate ligand. Styrenylation involves unfavourable palladacycle ring strain such that its direct *β*-hydride elimination proceeds via the displacement of the directing group pyrimidinyl-N atom by the acetate ligand that subsequently binds via bidentate mode (**ts-5b**, 19.2 kcal mol^{-1}) rather than via the intact palladacycle with the acetate ligand bound in a monodentate fashion (**ts-5b-c2**) (Figure S17). As a result, to form the styrenyl product the rotational barrier became the overall regio-determining step and this required a very high barrier as the palladacycle experienced huge strain when H_s was brought to interact agostically with Pd(II) centre (Figure S18(ii)).

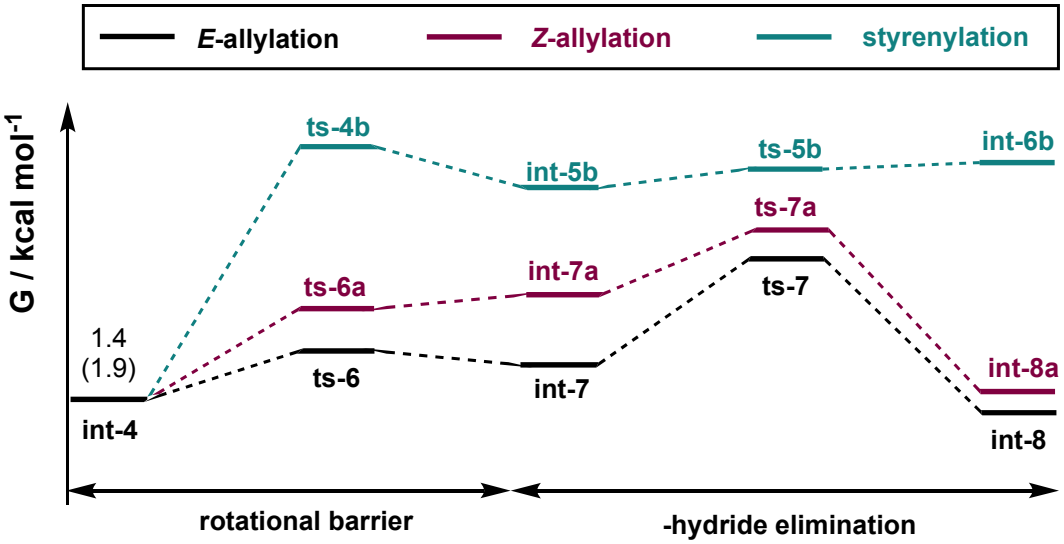

Reaction product	direct β-H elimination				ligand-promoted β-H elimination				Overall barrier [a]
	ts-4x	int-5x	ts-5x	int-6x	ts-6x	int-7x	ts-7x	int-8x	
E-allyl (**x=nil**)	15.0‡ (14.9‡)	12.4 (12.7)	15.6‡ (15.3‡)	8.5 (8.4)	4.3‡ (4.7‡)	3.8 (6.0)	**9.2‡ (10.7‡)**	-0.4 (-0.3)	**7.8 (8.8)**
Z-ally (**x=a**)	16.8‡ (16.5‡)	14.7 (15.1)	17.6‡ (17.6‡)	9.6 (10.0)	5.9‡ (6.4‡)	7.0 (8.9)	**11.3‡ (12.7‡)**	0.7 0.6	**9.9 (10.8)**
styrenyl (**x=b**)	**21.0‡, [b] (21.8‡)**	17.9 (18.7)	19.2‡, [c] (19.2‡)	20.4 (18.3)	**21.0‡, [b] (21.8‡)**	3.9 (4.7)	48.5‡ (48.3‡)	10.5 (8.3)	**19.6 (19.9)**

[a] We take the lowest value of the two. Both *E*- and *Z*-allylation preferred acetate-promoted β-hydride elimination, whereas styrenylation preferred direct β-hydride elimination via Pd(II) hydride complex.

[b] Rotational TS for styrenylation are the same regardless of whether β-hydride elimination occurs directly or via ligand involvement. The prerequisite is to bring the H_s atom to interact agostically with Pd(II)-centre.

[c] The TS where the directing group got displaced (**ts-5b**) has a lower activation barrier than the one where it remains coordinated (**ts-5b-c2**) since the former released the unfavourable strain in the palladacycle.

Table S10. Gibbs energies for selectivity studies for *trans*-hexene. TDTS values are given in bold.

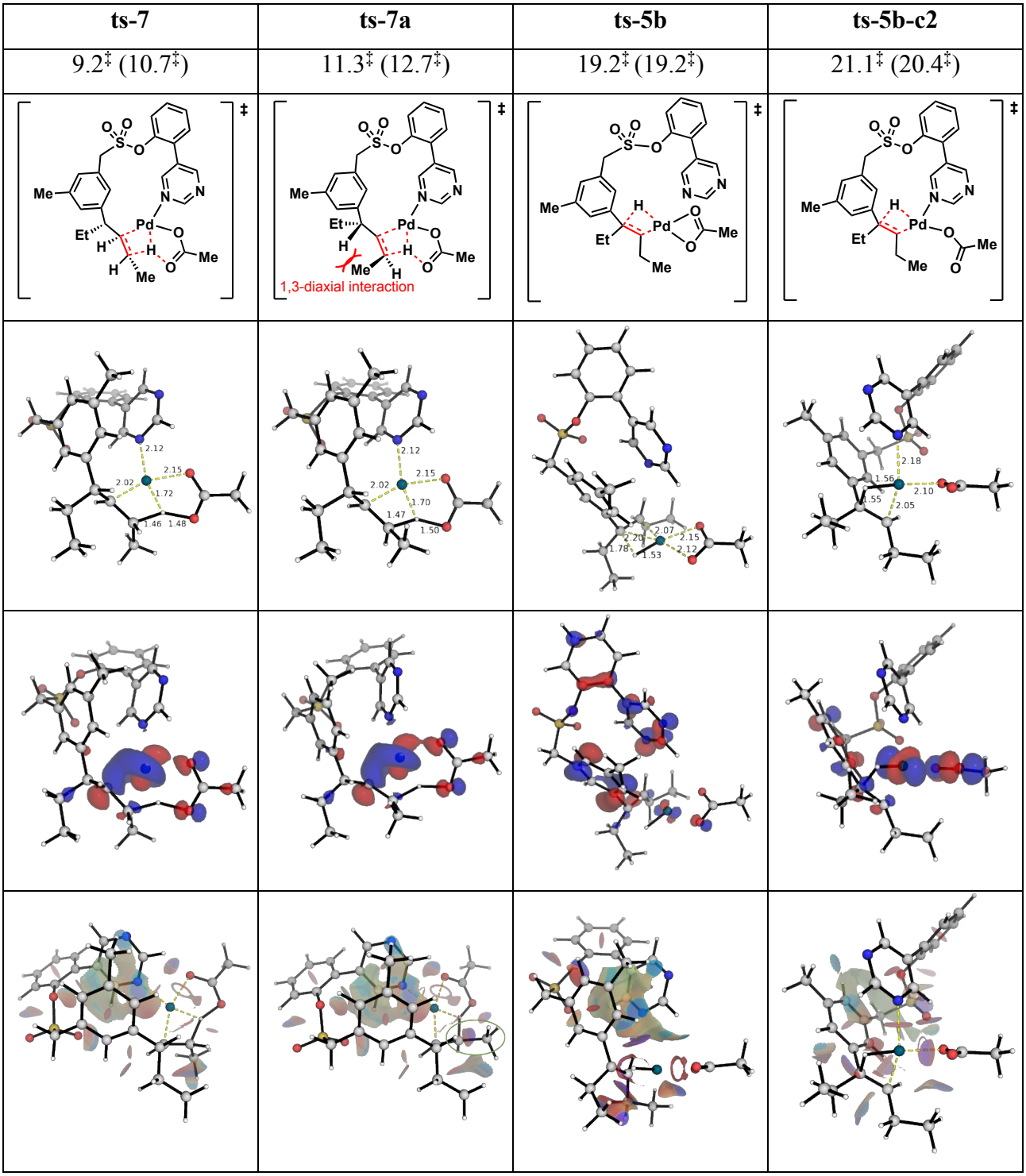

Figure S17. Product selectivity studies. The β-hydride elimination TSs for each product formation is given, with their HOMOs (isosurface value of 0.05) and NCI plots.

The dihedral angle scans allow us to compare the rotational barriers required to form allyl- vs styrenyl-product since the rotational barrier for the latter is regio-determining. We can see that styrenylation has a hugely disfavoured ring strain when the required H atom (H_s in Figure S18(ii)) is brought to interact agostically with Pd(II) centre – a prerequisite for the subsequent β-hydride elimination. Note that as discussed in the main text, the allylation involved steps that did not impose any strain on the 14-m palladacycle whereas the styrenylation severely distorted the palladacycle giving rise to hugely unfavourable ring strains.

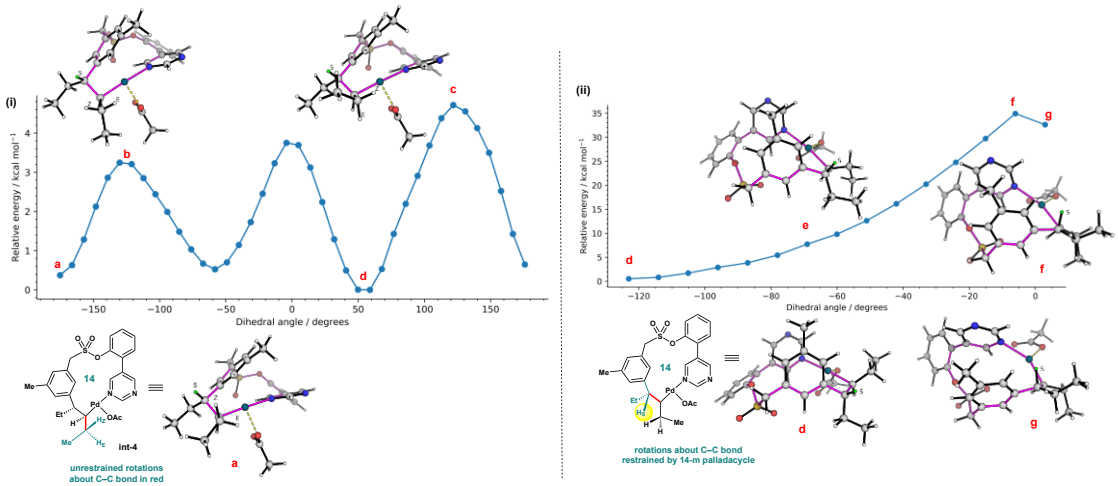

Figure S18. Dihedral angle scan (about C–C bond in red) for rotational barrier for the formation of (i) *E*-/*Z*-allylated products and (ii) styrenyl product for *trans*-hexene substrate. Note the different energy scales used. In (ii), note the position of styrenyl proton (H_s, labelled *S* in green), which is restrained in a position away from Pd(II)-centre by the conformationally rigid ring (outlined in purple).

2.9.6 Arene site-selectivity (HOMO, NCI plots and isodesmic studies)

The *ortho*-/*para*-positions on the arene for potential activation were compared to *meta*-activation. The C–H activation and 1,2-migratory insertion steps were studied. The comparative energies for the key steps were given in Table S11. For the turnover frequency determining step, *para*-insertion (**ts-3p**) was 3.9 kcal mol^{-1} higher in activation barrier than *meta*-insertion (**ts-3**), translating to 1 in 222 selectivity; *ortho*-insertion (**ts-3o**) was 12.7 kcal mol^{-1} higher than ts-3, making *ortho*-insertion uncompetitive (1 in 40 million). These agreed well with observed selectivities which can be traced to unfavorable sterics involved in *ortho*- and *para*-addition (Figure S19).

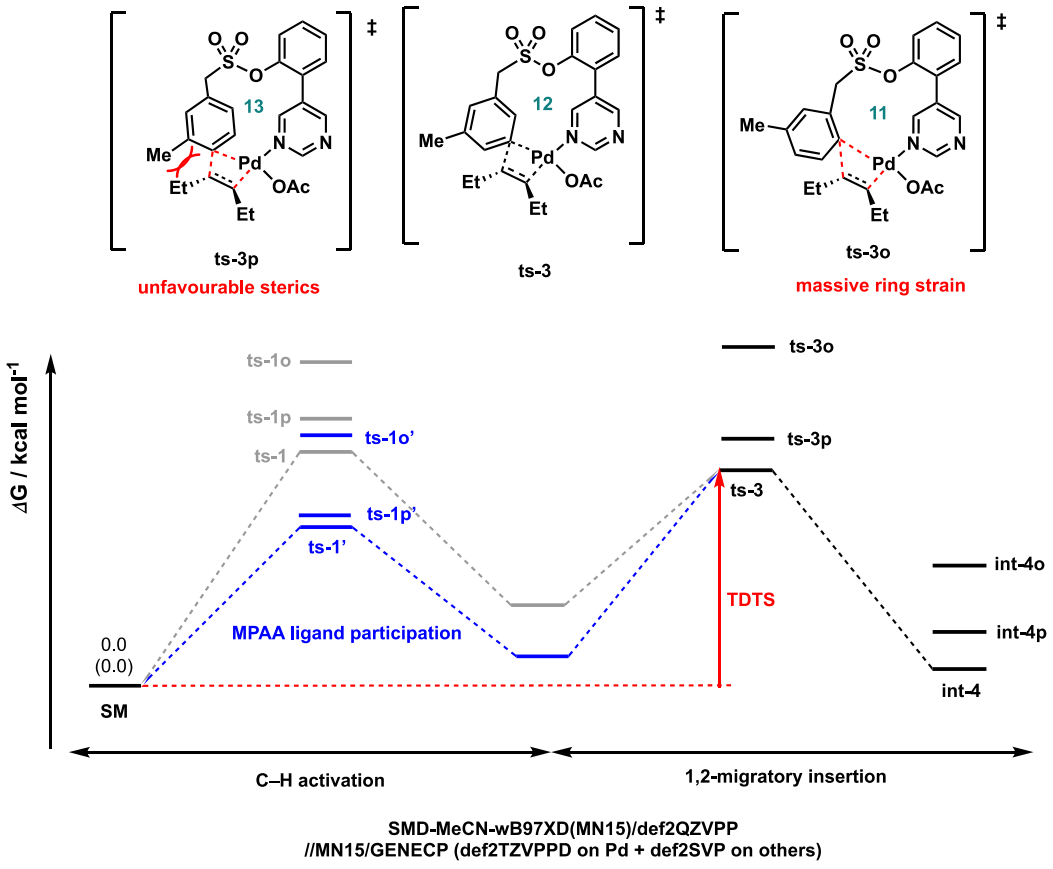

Allylation site	**ts-1x**	**ts-1x'**	**ts-3x**	**int-4x**
meta- **(x=nil)**	26.7‡ (28.2‡)	20.0‡ (20.8‡)	**23.2‡** **(23.8‡)**	1.4 (1.9)
ortho- **(x=o)**	35.8‡ (34.9‡)	28.7‡ (29.2‡)	**37.0‡** **(35.5‡)**	19.2 (18.2)
para- **(x=p)**	28.6‡ (28.6‡)	20.5‡ (20.0‡)	**28.2‡** **(26.7‡)**	8.4 (8.2)

Table S11| Arene site-selectivity studies. MPAA ligands lowered C–H activation in all cases such that 1,2- migratory insertion (ts-3x) becomes the TDTS whose barriers are given in bold.

In addition to the stereoelectronic effects associated with arene site selectivity, the ring strain energies in these TSs were calculated from the reaction enthalpy of the isodesmic reaction[19,20] shown in Scheme S2. Specifically, a hypothetical pyridine ligand was used for TS searches to release the ring strain where the directing group (DG) got uncoordinated. The starting conformation for the DG (highlighted in green, Scheme S2) in all 3 cases was made the same in a linear form for subsequent TS searches. The enthalpies of the reactions were further corrected with SMD solvation model: $\Delta H^{\ddagger}_{sol} = \Delta H^{\ddagger}_{gas} - \Delta E^{\ddagger}_{gas} + \Delta E^{\ddagger}_{sol}$. The calculations showed that the *meta*-insertion TDTS had the lowest ring strain at 0.3 kcal mol^{-1}, followed by *para*-insertion TDTS, with 4.7 kcal mol^{-1}; *ortho*-insertion TDTS had the largest ring strain at 12.1 kcal mol^{-1}. These values are in excellent quantitative agreement with the selectivity studies (Table S11, where *para*-TDTS is about 4 kcal mol^{-1} and *ortho*-TDTS is about 12 kcal mol^{-1} higher than *meta*-TDTS).

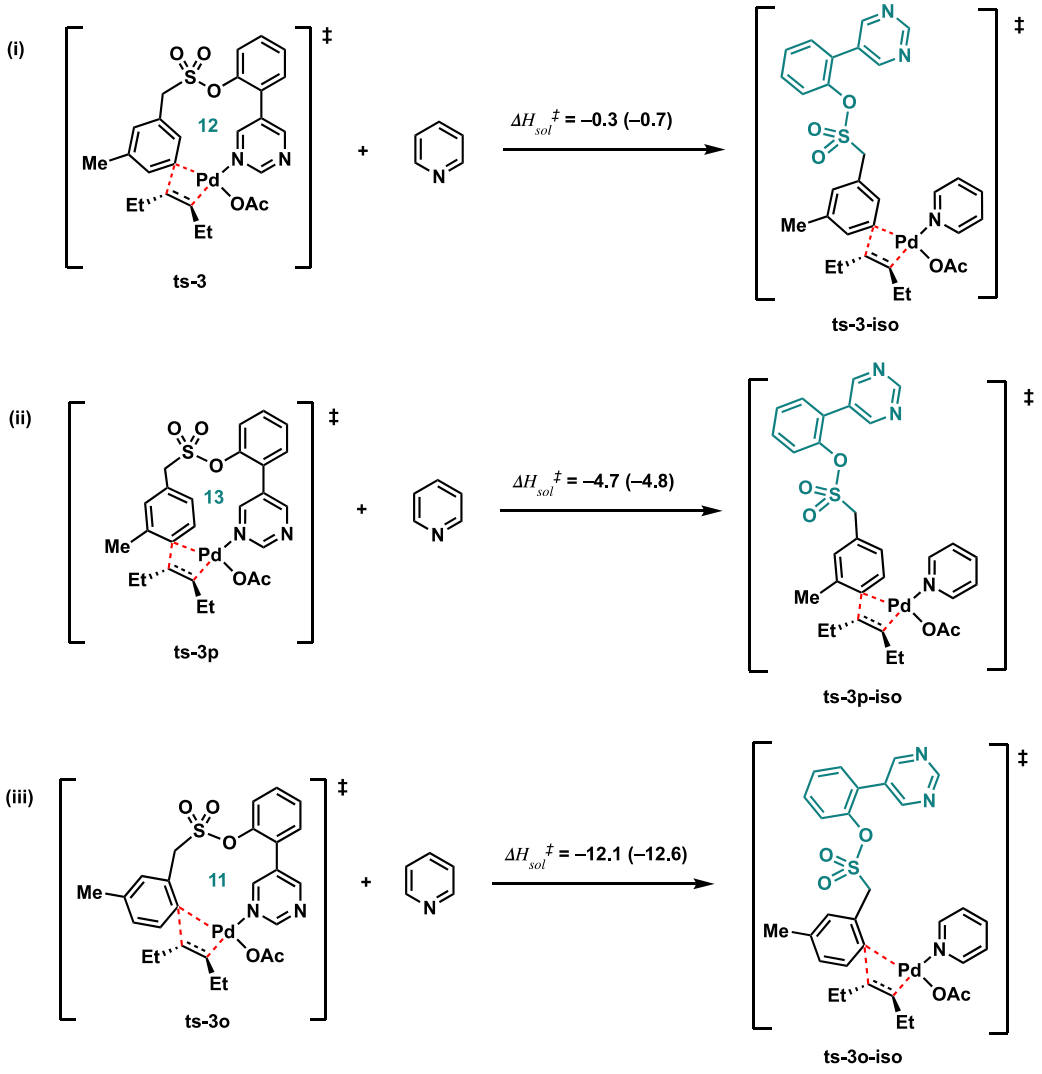

Scheme S2. Computed ring strain energies by study of isodesmic reaction where a hypothetical pyridine ligand is involved. Enthalpies quoted are corrected with solvent effect and in kcal mol^{-1}.

The HOMOs for insertion TDTSs for *meta*-/*ortho*-/*para*-activation were plotted in Figure S19 Top. These show similar electron distributions, suggesting that electronic factors are less important in the selectivity of arene site activation. NCI plots (Figure S19 Bottom) show that **ts-3p** was sterically disfavoured when the methyl-group on the ring came close to the alkene being added whereas in **ts-3o**, the excessive ring strain made this TS highly strained (the directing group got twisted out of shape), giving rise to unfavourably high activation barrier. The possibility of addition to the other *ortho*-site would bring the methyl-group into close proximity of the alkene being added, further increasing the activation strain and was thus not considered.

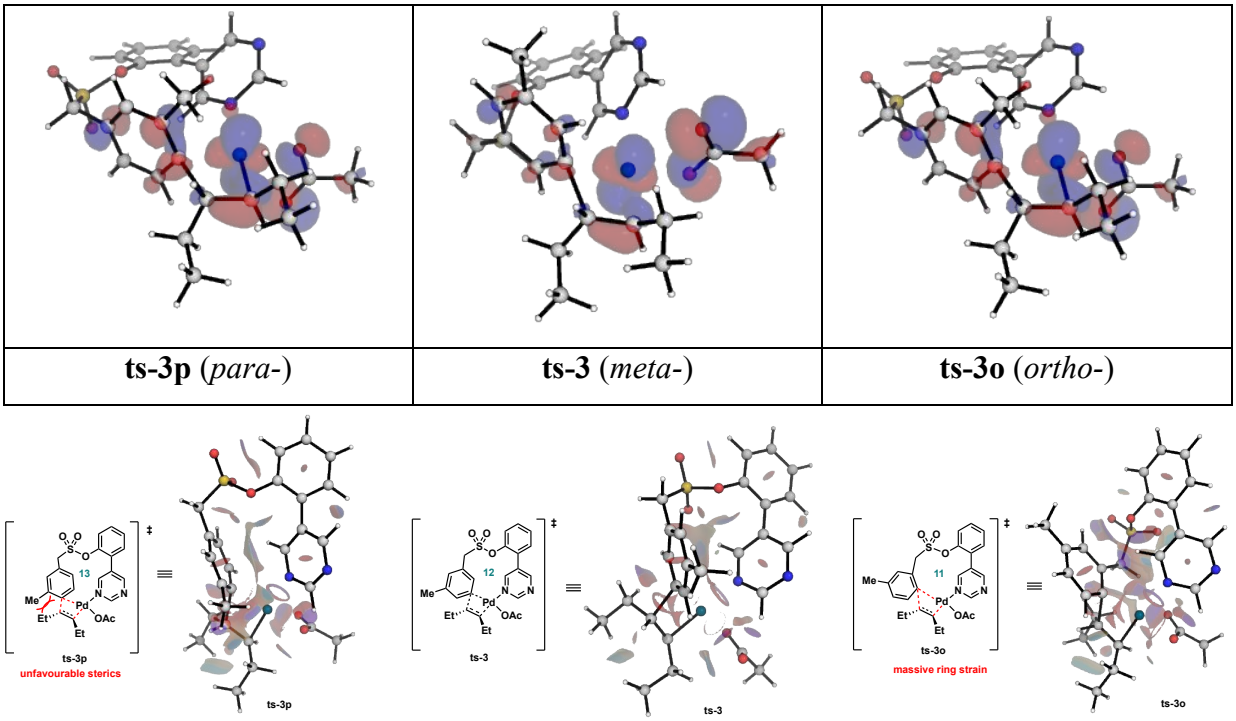

Figure S19. Insertion TSs from *para*-, *meta*- and *ortho*-activated complexes. Top: HOMOs at an isovalue of 0.04. Bottom: NCI plots.

2.9.7 General conformational sampling of TDTSs (1,2-migratory insertion step)

Once a TS was found, the structure was used as starting guesses for searching TS conformers. The palladacycle ring was frozen and rotamers along C–C bonds in red (Scheme S3) were generated for TS conformational searches. Altogether, 9 TSs were found for each orientation of alkene (18 TSs for each of *trans*-hexene and *cis*-hexene) and 4 TSs were found for each orientation of cyclohexene (8 TSs altogether). The optimized TS structures and their relative energy barriers with respect to the lowest barrier TS for *trans*-hexene substrate ($\Delta\Delta G^{\neq}$) were shown in Figure S20.

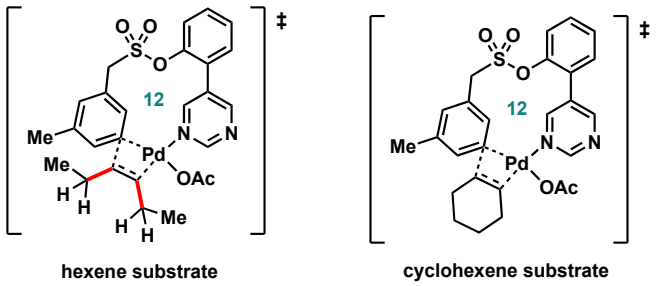

Scheme S4. Rotamers were generated by varying the dihedral angles in red in conformational sampling of the 1,2-migratory insertion TDTSs for *trans*- and *cis*-hexene substrates; for cyclohexene substrate, the buckling of the half-chair in different orientations were considered.

Boltzmann weighting and selectivity

All TDTS conformers were used for Boltzmann weighting to give selectivity ratio. Standard procedures for Boltzmann weighting were applied (see, for example, Equation (2) of ref. [21] and SI of ref. [22]); specifically, the selectivity between two products A and B were calculated *via*

$$\frac{[\mathrm{A}]}{[\mathrm{B}]} = \frac{\sum_{i\,\in\,all\ confs,A}^{N} e^{-\Delta\Delta G^{\neq}_{0i,A}/RT}}{\sum_{j\,\in\,all\ confs,B}^{N} e^{-\Delta\Delta G^{\neq}_{0j,B}/RT}} \qquad (1)$$

where $\Delta\Delta G^{\neq}_{0i,X} = \Delta G^{\neq}_{i,X} - \Delta G^{\neq}_{0,X}$ is the energy difference between the i^{th} conformer of product X (X = A, B) and the lowest energy conformer of all products, state 0.

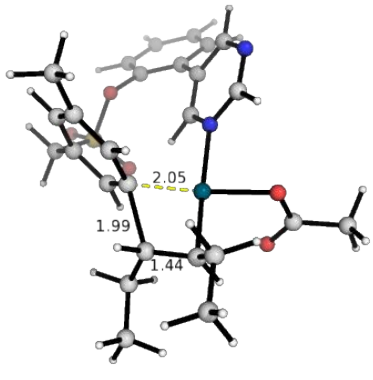	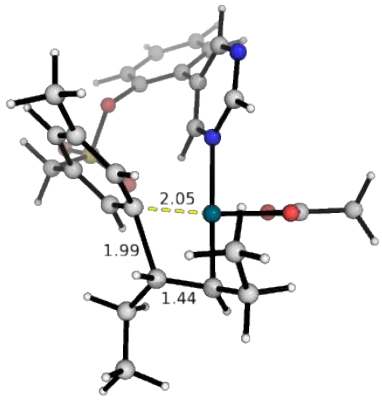	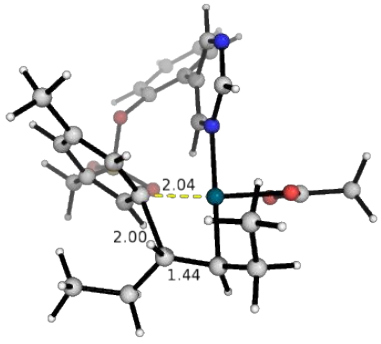
$\Delta\Delta G^{\neq} = 1.2\ (1.3)$	$\Delta\Delta G^{\neq} = 1.3\ (1.1)$	$\Delta\Delta G^{\neq} = 2.4\ (1.7)$
***trans*-d1-c1**	***trans*-d1-c2**	***trans*-d1-c3**

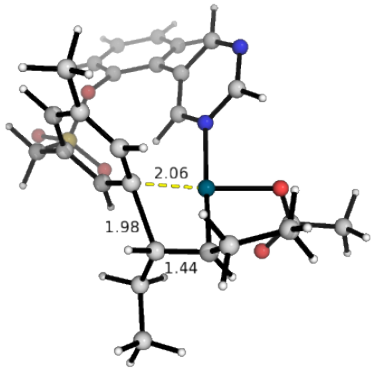	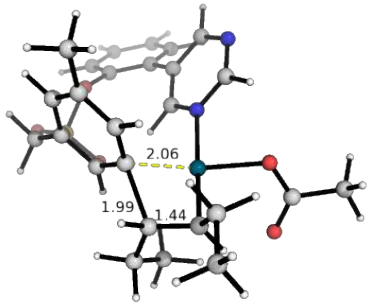	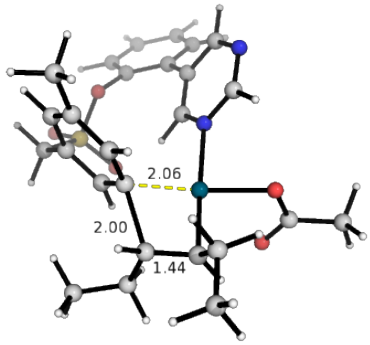
$\Delta\Delta G^{\neq} = 2.6$ (2.6)	$\Delta\Delta G^{\neq} = 2.9$ (2.5)	$\Delta\Delta G^{\neq} = 2.9$ (3.5)
***trans*-d1-c4**	***trans*-d1-c5**	***trans*-d1-c6**
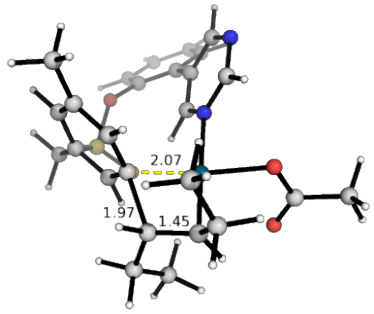	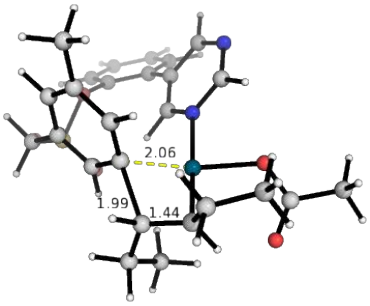	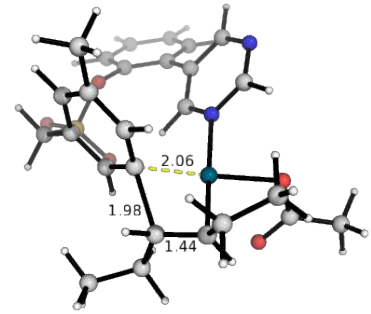
$\Delta\Delta G^{\neq} = 3.3$ (2.4)	$\Delta\Delta G^{\neq} = 3.7$ (3.0)	$\Delta\Delta G^{\neq} = 5.2$ (4.6)
***trans*-d1-c7**	***trans*-d1-c8**	***trans*-d1-c9**

(a) Conformers for 1,2-migratory insertion TDTS for diastereomer 1 (d1) formation from *trans*-hexene.

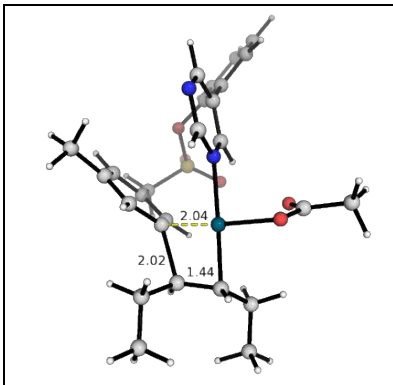	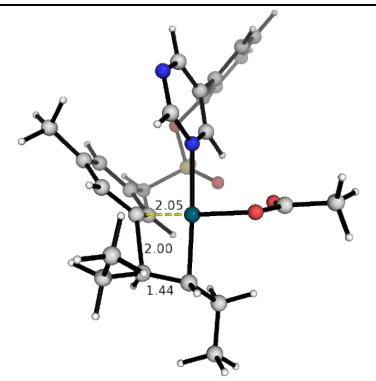	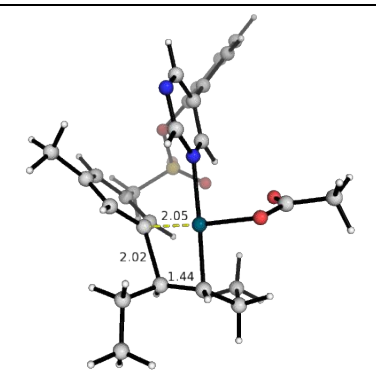
$\Delta\Delta G^{\neq} = 0.0$ (0.0)	$\Delta\Delta G^{\neq} = 0.6$ (0.4)	$\Delta\Delta G^{\neq} = 1.2$ (0.9)

***trans*-d2-c1**	***trans*-d2-c2**	***trans*-d2-c3**
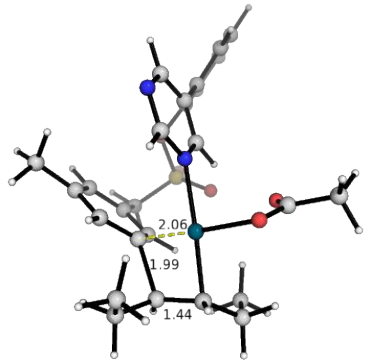	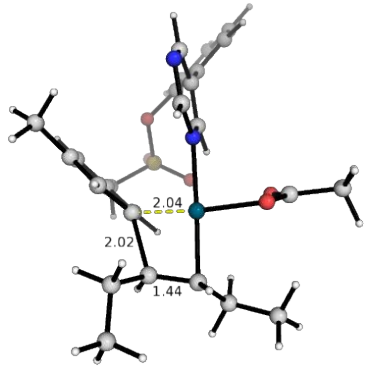	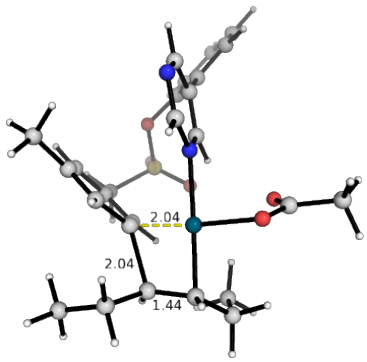
$\Delta\Delta G^{\neq} = 2.0\ (1.3)$	$\Delta\Delta G^{\neq} = 2.2\ (2.4)$	$\Delta\Delta G^{\neq} = 2.4\ (2.1)$
***trans*-d2-c4**	***trans*-d2-c5**	***trans*-d2-c6**
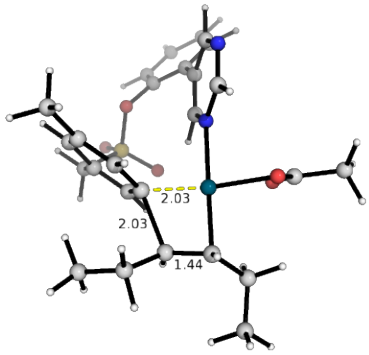	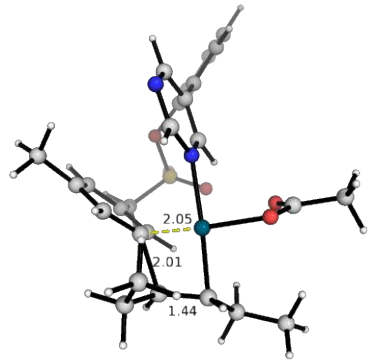	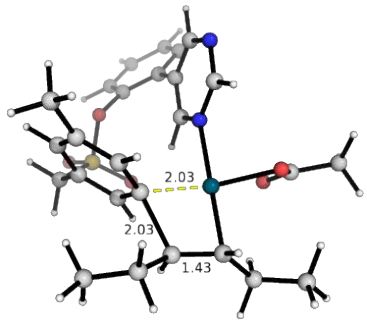
$\Delta\Delta G^{\neq} = 2.6\ (2.1)$	$\Delta\Delta G^{\neq} = 2.6\ (1.9)$	$\Delta\Delta G^{\neq} = 4.5\ (4.0)$
***trans*-d2-c7**	***trans*-d2-c8**	***trans*-d2-c9**

(b) Conformers for 1,2-migratory insertion TDTS for diastereomer 2 (d2) formation from *trans*-hexene.

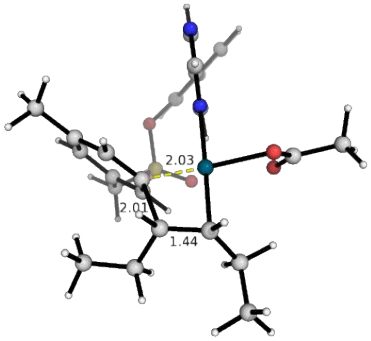	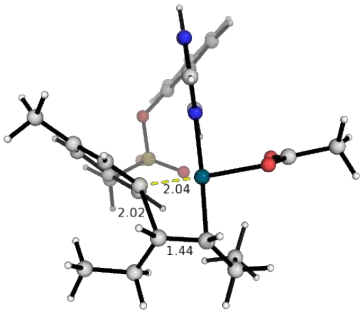	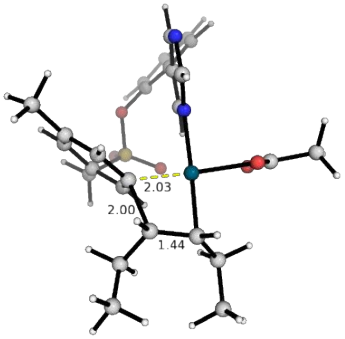
$\Delta\Delta G^{\neq} = 0.3\ (-0.2)$	$\Delta\Delta G^{\neq} = 1.0\ (0.6)$	$\Delta\Delta G^{\neq} = 1.2\ (1.0)$
***cis*-d1-c1**	***cis*-d1-c2**	***cis*-d1-c3**
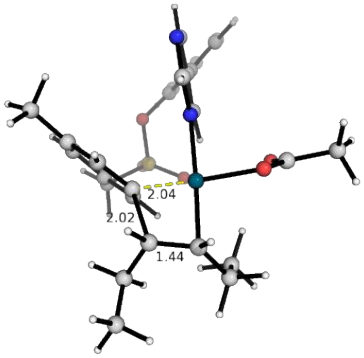	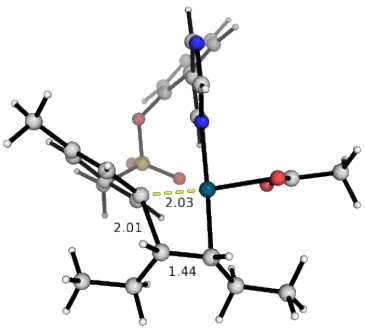	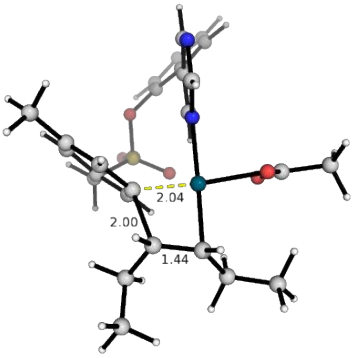
$\Delta\Delta G^{\neq} = 1.2\ (1.2)$	$\Delta\Delta G^{\neq} = 1.7\ (0.8)$	$\Delta\Delta G^{\neq} = 2.5\ (2.1)$
***cis*-d1-c4**	***cis*-d1-c5**	***cis*-d1-c6**
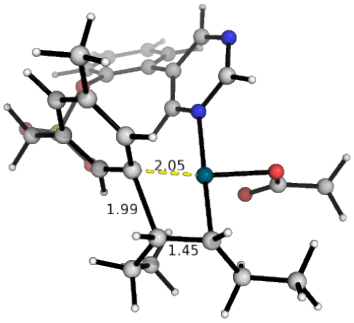	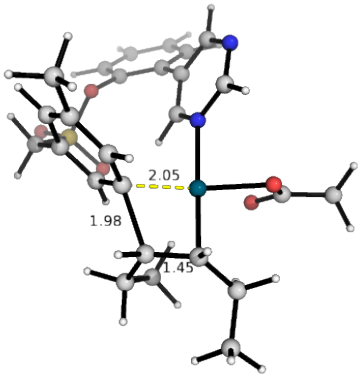	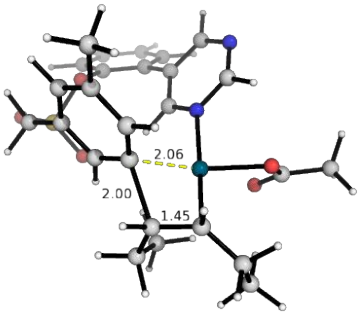
$\Delta\Delta G^{\neq} = 5.8\ (4.5)$	$\Delta\Delta G^{\neq} = 5.8\ (4.8)$	$\Delta\Delta G^{\neq} = 10.9\ (9.7)$
***cis*-d1-c7**	***cis*-d1-c8**	***cis*-d1-c9**

(c) Conformers for 1,2-migratory insertion TDTS for diastereomer 1 (d1) formation from *cis*-hexene.

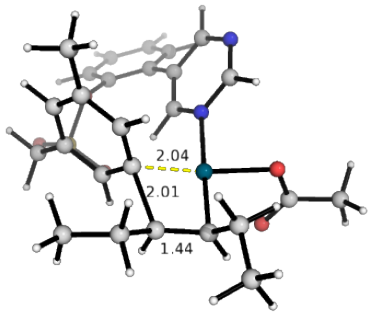	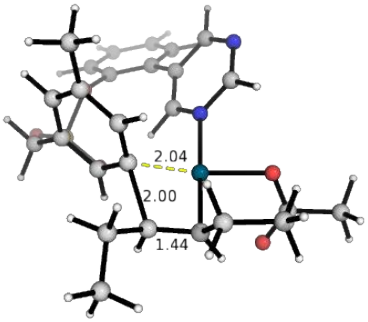	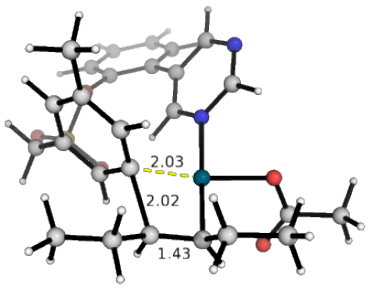
$\Delta\Delta G^{\neq} = 1.6\ (1.0)$	$\Delta\Delta G^{\neq} = 1.7\ (1.4)$	$\Delta\Delta G^{\neq} = 1.8\ (1.1)$
***cis*-d2-c1**	***cis*-d2-c2**	***cis*-d2-c3**
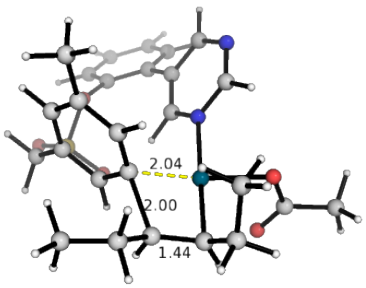	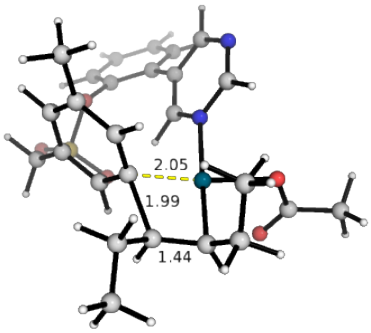	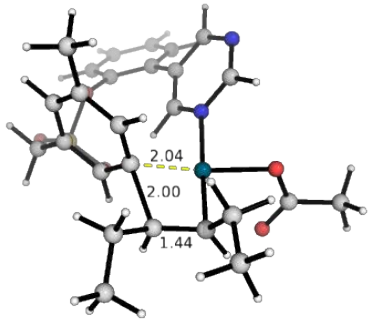
$\Delta\Delta G^{\neq} = 2.2\ (0.9)$	$\Delta\Delta G^{\neq} = 2.5\ (1.5)$	$\Delta\Delta G^{\neq} = 2.6\ (2.3)$
***cis*-d2-c4**	***cis*-d2-c5**	***cis*-d2-c6**
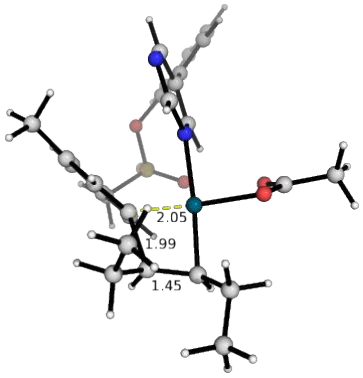	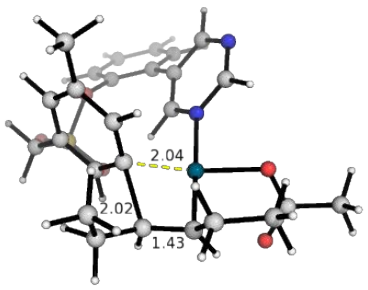	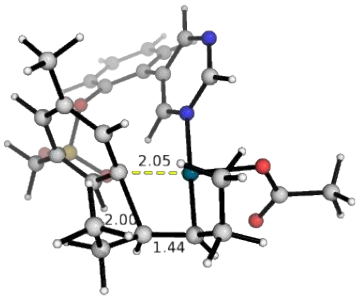
$\Delta\Delta G^{\neq} = 4.2\ (4.1)$	$\Delta\Delta G^{\neq} = 6.4\ (6.8)$	$\Delta\Delta G^{\neq} = 7.4\ (7.1)$
***cis*-d2-c7**	***cis*-d2-c8**	***cis*-d2-c9**

(d) Conformers for 1,2-migratory insertion TDTS for diastereomer 2 (d2) formation from *cis*-hexene.

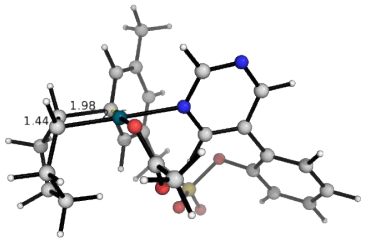	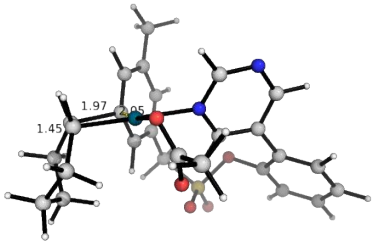	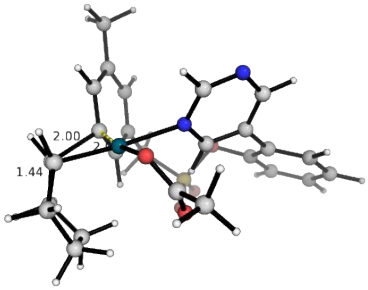
$\Delta\Delta G^{\neq} = 2.7$ (2.8)	$\Delta\Delta G^{\neq} = 3.3$(3.6)	$\Delta\Delta G^{\neq} = 4.5$ (3.7)
cy-d1-c1	**cy-d1-c2**	**cy-d1-c3**
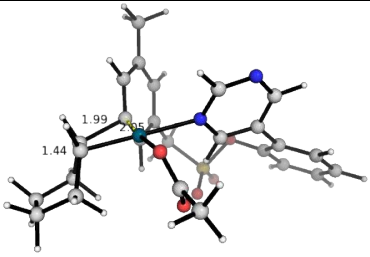		
$\Delta\Delta G^{\neq} = 5.2$ (5.0)		
cy-d1-c4		

(e) Conformers for 1,2-migratory insertion TDTS for diastereomer 1 (d1) formation from cyclohexene (cy).

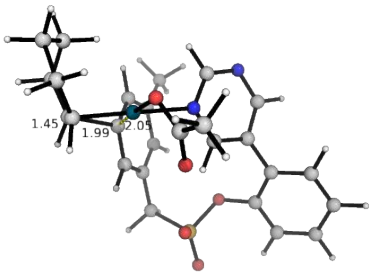	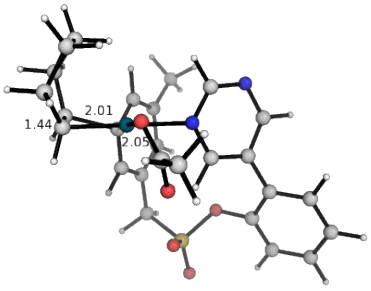	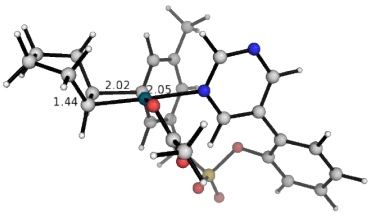
$\Delta\Delta G^{\neq} = 3.7$ (4.0)	$\Delta\Delta G^{\neq} = 4.3$ (3.3)	$\Delta\Delta G^{\neq} = 4.4$ (4.6)
cy-d2-c1	**cy-d2-c2**	**cy-d2-c3**

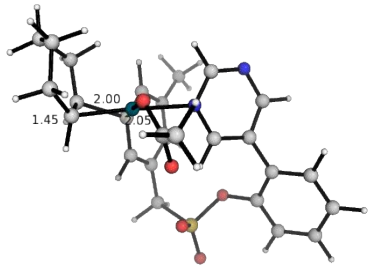		
$\Delta\Delta G^{\neq} = 4.4\ (4.8)$		
cy-d2-c4		

(f) Conformers for 1,2-migratory insertion TDTS for diastereomer 2 (d2) formation from cyclohexene (cy).

Figure S20. Optimized TS geometries for 1,2-migratory insertion TDTS step for *trans*-hexne (a and b), *cis*-hexene (c and d) and cyclohexene (e and f). All TSs were taken relative to the same minima (*trans*-d2-c1). Relative $\Delta\Delta G^{\neq}$ values are in kcal mol^{-1}. Bond lengths are given in Angstroms.

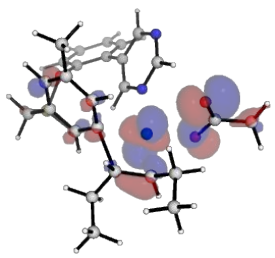	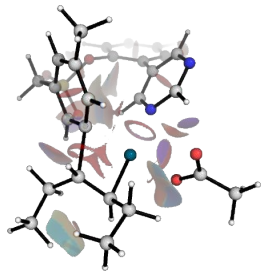	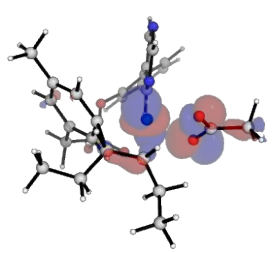	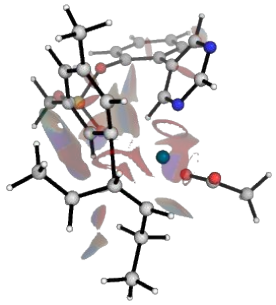
(i)		(ii)	

Figure S21. HOMO (isosurface value of 0.04) and NCI plots for the 1,2-migrator insertion TDTS lowest barrier conformer for (i) *trans*-hexene and (ii) *cis*-hexene. The comparisons show that stereoelectronics are rather similar, suggesting similar reactivities.

2.9.8 Product selectivity studies for *cis*-hexene substrate

Following from results using *trans*-hexene (section 2.9.5), the lowest pathways for *cis*-hexene product selectivity were studied and the key TS structures shown. Here again, for styrenylation, the TS where the DG got displaced (***cis*-ts-5b** at 16.1‡ (15.3‡) kcal mol^{-1}) has a lower activation barrier than the one where it remained coordinated (***cis*-ts-5b-c2** at 23.1‡ (22.5‡) kcal mol^{-1}) since the former released the unfavourable strain in the palladacycle (Figure S22).

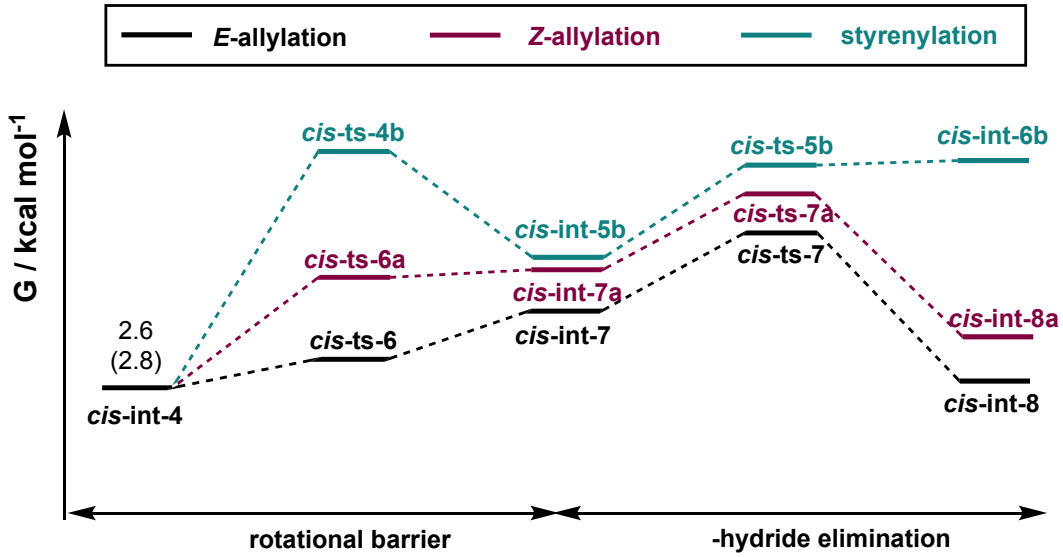

Reaction product	direct β-H elimination				ligand-promoted β-H elimination				Overall barrier
	cis-ts-4x	*cis*-int-5x	*cis*-ts-5x	*cis*-int-6x	*cis*-ts-6x	*cis*-int-7x	*cis*-ts-7x	*cis*-int-8x	
E-allyl (**x=nil**)	–	–	–	–	4.9‡ (5.1‡)	10.8 (10.5)	**13.8‡ (14.9‡)**	3.5 (3.0)	**11.2 (12.1)**
Z-ally (**x=a**)	–	–	–	–	10.7‡ (11.4‡)	11.7 (13.3)	**17.4‡ (18.6‡)**	7.1 (6.4)	**14.8 (15.8)**
styrenyl (**x=b**)	**20.8‡ (22.2‡)**	11.7 (12.3)	16.1‡ (15.3‡)	17.1 (14.8)	–	–	–	–	**18.2 (19.4)**

Table S11. Gibbs energies for selectivity studies for *cis*-hexene. TDTS values are given in bold.

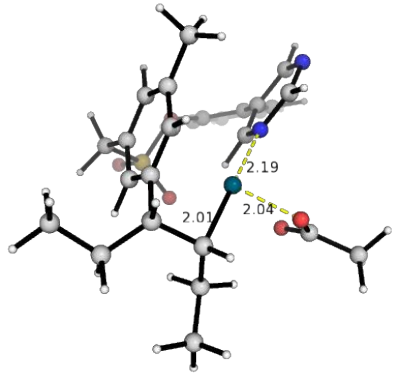	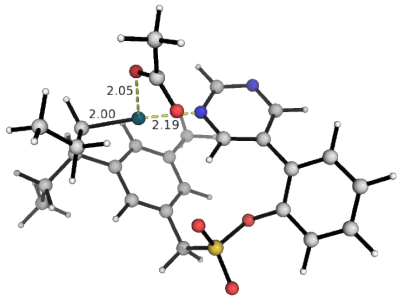	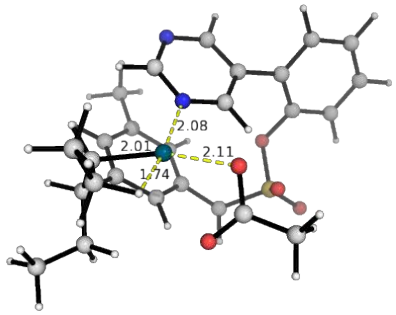
***cis*-int-4**	***cis*-ts-6**	***cis*-int-7**
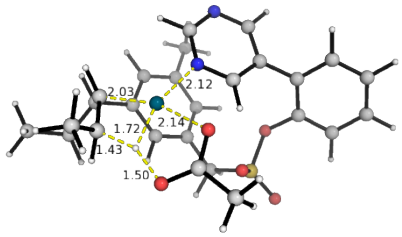	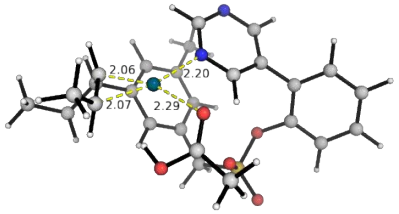	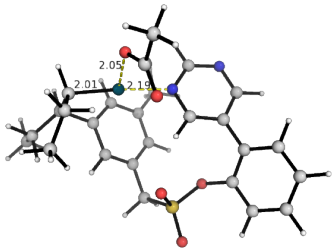
***cis*-ts-7**	***cis*-int-8**	***cis*-ts-6a**
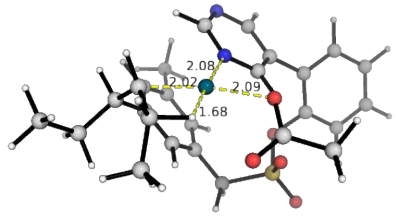	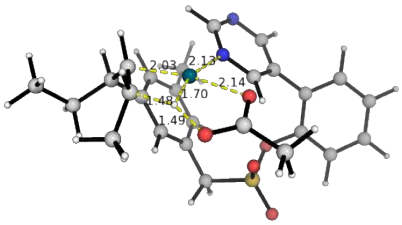	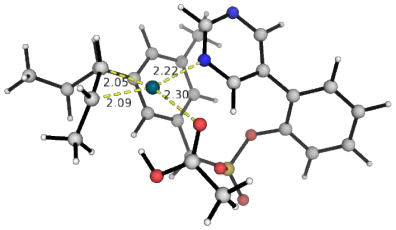
***cis*-int-7a**	***cis*-ts-7a**	***cis*-int-8a**
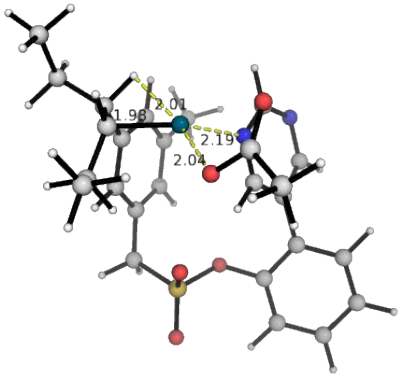	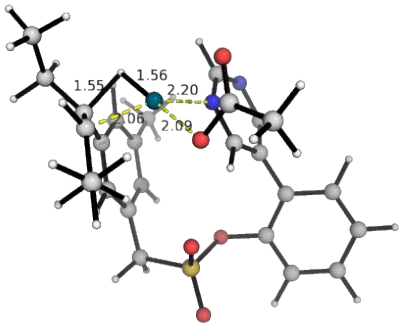	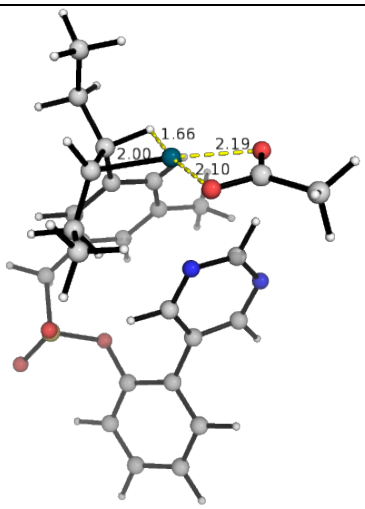
***cis*-ts-4b**	***cis*-ts-5b-c2**	***cis*-int-5b**

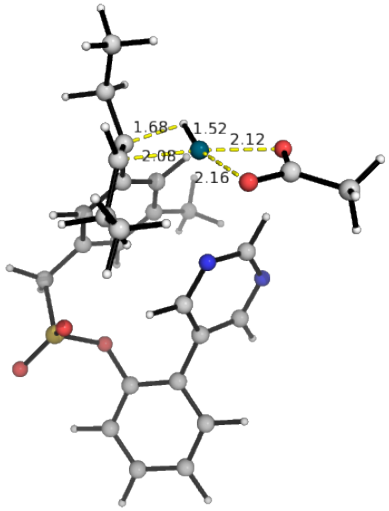	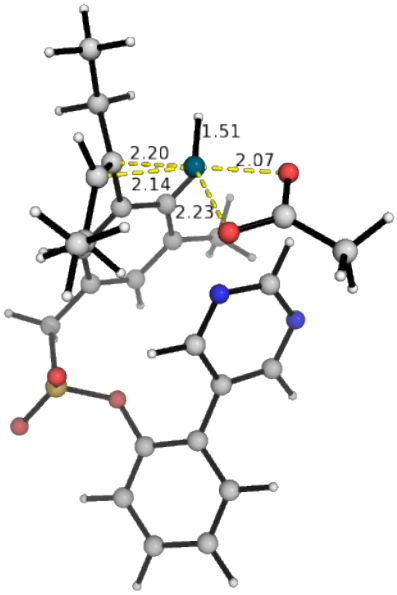	
***cis*-ts-5b**	***cis*-int-6b**	

Figure S22. Optimised TS structures for selectivity studies using *cis*-hexene substrate.

HOMOs for ligand-assisted β-H elimination for both allylation using *cis*-hexene substrate (Figure S23) are similar to each other and similar to those for *trans*-hexene (Figure S17), where a σ^*_{CC} bond is broken and a π_{CC} bond is formed as the deprotonation occurred. The differences in the *E*-/*Z*-allylation stereoselectivity could arise due to the slightly less favourable NCIs in *Z*-allylation (Figure S23).

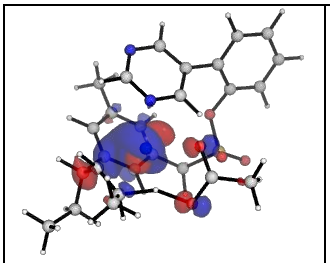	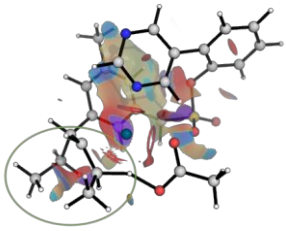	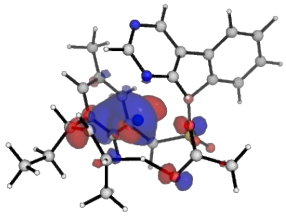	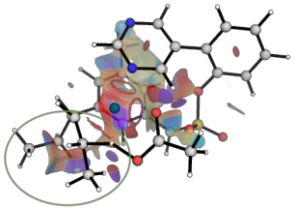
***cis*-ts-7 (*E*-allylation)**		***cis*-ts-7a (*Z*-allylation)**	

Figure S23. HOMOs (isosurface value 0.05) and NCI plots for *E*- vs *Z*-allylated product selectivity for *cis*-hexene substrate.

Although for allylation, the ligand-assisted β-H elimination is the r.d.s. for product selectivity, the rotational barrier to bring the H_s atom to interact agostically with Pd(II) centre before direct β-H elimination is the r.d.s. for styrenylation. A comparison between such rotations by the dihedral angle scans along key C–C bonds can be instructive (Figure S24).

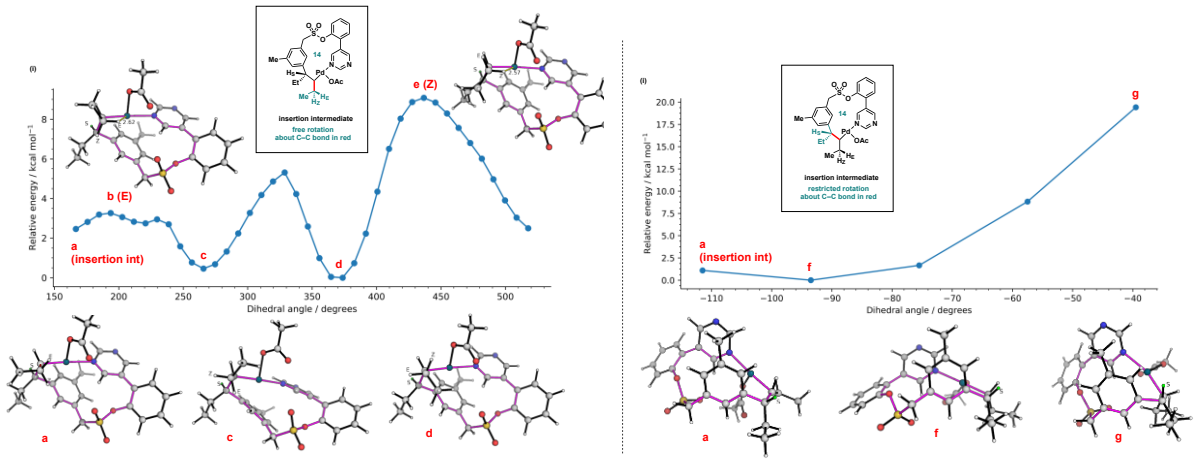

Figure S24. Dihedral angle scan (about C–C bond in red) for rotational barrier for the formation of (i) *E*-/*Z*-allylated products and (ii) styrenyl product for *cis*-hexene substrate. Note the different energy scales used. In (ii), the position of styrenyl proton (H_s, labelled *S* in green) is restrained away from Pd(II)-centre by the conformationally rigid ring (outlined in purple).

2.9.9 Product selectivity studies for cyclohexene substrate

Initial dihedral angle scans were performed about the key C–C bonds to locate rotational barriers bringing the H atom (for subsequent β-H elimination) to interact agostically with Pd(II)-centre (Figure S25). Only rotational barriers for *Z*-allylation could be located; both *E*-allylation and styrenylation had rotational barriers that were about 30 kcal mol^{-1} higher than for *Z*-allylation; these arise due to unfavourable ring distortions imposed by the rigid cyclohexyl ring fused to the rigid palladacycle in the insertion intermediate. The overall Gibbs energy profile for cyclohexene substrate were shown in Figure S26. Given that the subsequent ligand-assisted β-H elimination for *Z*-allylation (**cy-ts-7a**) was 6.3 kcal mol^{-1} higher than the rotational barrier (**cy-ts-6a**), we estimate

that the barriers for both *E*-allylation and styrenylation are at least ~20 kcal mol^{-1} higher than *Z*-allylation (**cy-ts-7a**), thus being disfavoured by 1 in a trillion. Therefore, if at all, only *Z*-allylated product can be formed using cyclohexene substrate.

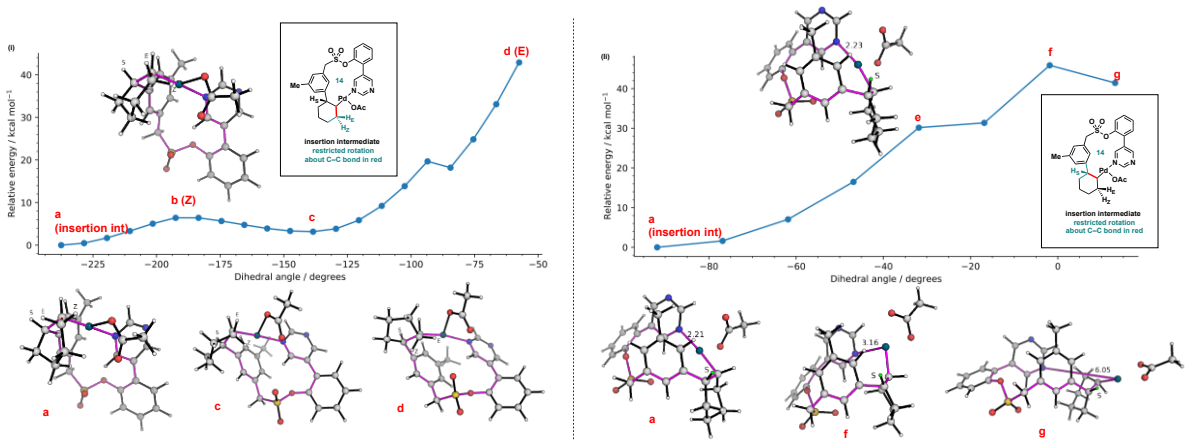

Figure S25. Dihedral angle scan (about C–C bond in red) for rotational barrier for the formation of (i) *E*-/*Z*-allylated products and (ii) styrenyl product for cyclohexene substrate.

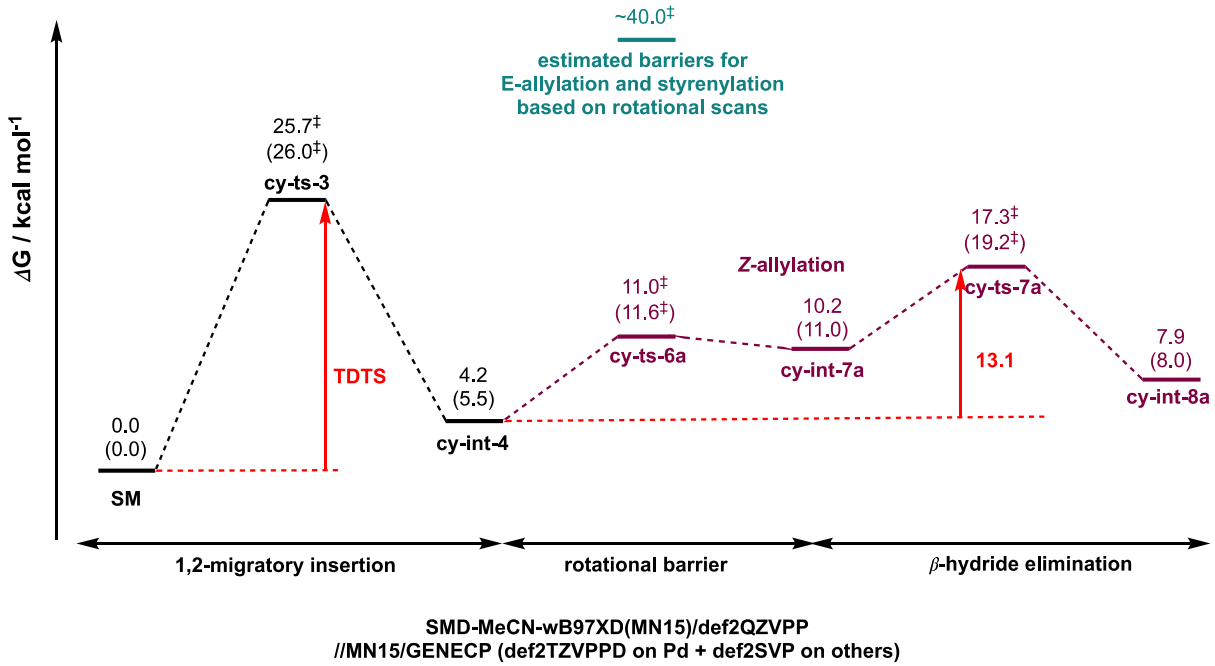

Figure S26. Gibbs free energy profile for *Z*-allylation using cyclohexene substrate. **cy-ts-3** is the same as **cy-d1-c1** as in Figure S20(e).

2.9.10 Absolute energies, zero-point energies

Absolute values (in Hartrees) for SCF energy, zero-point vibrational energy (ZPE), enthalpy and quasi-harmonic Gibbs free energy (at 363K) for optimised structures are given below. For harmonic frequency analysis, a plus (+) sign indicates that the lowest frequency of the optimised energy minimal structures is positive, and single negative frequency for each transition state is included. Single point corrections in SMD acetonitrile using ωB97X-D and MN15 functionals are also included. Each sub-heading corresponds to a subfolder inside the *structures_xyz* folder where all optimised structural coordinates are given in *.xyz* format, along with the corresponding (gas-phase) energy, *E*.

Structure	E/au	ZPE/au	H/au	qh-G/au	Im.Freq/ cm^{-1}	SP ωB97X-D (MeCN)	SP MN15 (MeCN)
0. Starting materials:							
arene 1a	-1426.5229	0.311509	-1426.1807	-1426.269	+	-1429.06227216	-1428.6919715
***trans*-hexene**	-235.31399	0.16511	-235.13645	-235.18577	+	-235.88622142	-235.7628220
***cis*-hexene**	-235.31226	0.165429	-235.13446	-235.18352	+	-235.88455969	-235.7610397
cyclo-hexene	-234.12832	0.146325	-233.97273	-234.01466	+	-234.68105898	-234.5687484

HOAc	-228.64453	0.062197	-228.57502	-228.61242	+	-229.13726389	-229.0706003
***N*-acetyl-norleucine**	-593.15819	0.231435	-592.90548	-592.97546	+	-594.47065223	-594.2582931
$Pd(OAc)_2$	-583.80993	0.104326	-583.69012	-583.74848	+	-585.03620367	-584.6482919
$Pd_3(OAc)_6$	-1751.5873	0.317868	-1751.2218	-1751.3472	+	-1755.21537801	-1754.0473816
1. *meta*-allylation:							
int-1	-2010.361	0.417336	-2009.8966	-2010.0187	+	-2014.12074330	-2013.3624531
ts-1	-2010.3361	0.411975	-2009.8774	-2009.9989	-1136.100	-2014.09487408	-2013.3327515
int-2	-2010.3515	0.417256	-2009.8868	-2010.0103	+	-2014.11044997	-2013.3506657

int-1'	-2146.2068	0.522938	-2145.6315	-2145.763	+	-2150.30584854	-2149.465115
ts-1'	-2146.1909	0.517866	-2145.6212	-2145.7518	-1275.1147	-2150.28508610	-2149.445114
int-2'	-2146.2152	0.523642	-2145.6392	-2145.771	+	-2150.30936515	-2149.472983
int-3	-2017.0314	0.521084	-2016.458	-2016.5904	+	-2020.87263588	-2020.0563355
ts-3	-2017.0153	0.52024	-2016.4439	-2016.5742	-281.0309	-2020.85715946	-2020.04
int-4	-2017.0546	0.522503	-2016.481	-2016.6102	+	-2020.89515397	-2020.078034
ts-4	-2017.0395	0.52057	-2016.4685	-2016.5959	-95.8045	-2020.87256581	-2020.056365
int-5	-2017.0424	0.520722	-2016.4705	-2016.5995	+	-2020.87613345	-2020.059231

ts-5	-2017.0376	0.518443	-2016.4684	-2016.5963	-534.1546	-2020.86947612	-2020.053557
int-6	-2017.0487	0.51989	-2016.4775	-2016.6068	+	-2020.88145514	-2020.065211
int-7	-2017.0479	0.520931	-2016.4759	-2016.6053	+	-2020.88962226	-2020.069785
ts-7	-2017.043	0.516919	-2016.4754	-2016.6038	-960.7952	-2020.87758394	-2020.058839
int-8	-2017.0651	0.521465	-2016.492	-2016.6228	+	-2020.89597912	-2020.079392
ts-7'	-2017.0165	0.516398	-2016.4485	-2016.579	-975.0604	-2020.84680381	-2020.030891
2. Regioselectivity (*Z*-allylation vs styrenylation):							
ts-4a	-2017.0372	0.521116	-2016.4659	-2016.5927	-77.2317	-2020.87072244	-2020.05477
int-5a	-2017.0391	0.521107	-2016.4669	-2016.5956	+	-2020.87307361	-2020.056043

ts-5a	-2017.0339	0.518458	-2016.4648	-2016.5926	-516.2140	-2020.86630718	-2020.049971
int-6a	-2017.0456	0.519994	-2016.4743	-2016.6036	+	-2020.87970642	-2020.062662
ts-7a	-2017.0403	0.517241	-2016.4725	-2016.6006	-912.4642	-2020.87472779	-2020.056175
ts-4b	-2017.0195	0.520651	-2016.4483	-2016.5763	-49.4039	-2020.86277303	-2020.045129
int-5b	-2017.023	0.52038	-2016.4513	-2016.5812	+	-2020.86634486	-2020.04869
ts-5b	-2017.0233	0.517549	-2016.4542	-2016.5852	-244.3729	-2020.86046599	-2020.044136
int-6b	-2017.0272	0.518973	-2016.4564	-2016.5874	+	-2020.86030520	-2020.047355
ts-7b	-2016.9853	0.513883	-2016.4199	-2016.5499	-1493.0469	-2020.81104238	-2019.995037

3. Ligand identity in TDTS:

ts-3-Ac-c1	-2017.01535	0.52024	-2016.44389	-2016.57418	-281.03090	-2020.85716	-2020.03997
ts-3-Ac-c2	-2017.01291	0.52006	-2016.44155	-2016.57193	-286.48340	-2020.85668	-2020.03961
ts-3-Ac-c3	-2017.01098	0.52017	-2016.43944	-2016.57063	-284.03240	-2020.85518	-2020.03759
ts-3-Ac-c4	-2017.01257	0.52013	-2016.44108	-2016.57153	-305.70220	-2020.85540	-2020.03868
ts-3-Ac-c5	-2017.00208	0.52015	-2016.43087	-2016.56047	-296.08770	-2020.85451	-2020.03664
ts-3-Ac-c6	-2017.00234	0.52011	-2016.43116	-2016.56056	-295.28320	-2020.85081	-2020.03394
ts3'_b-aa-c1	-2381.5373	0.689422	-2380.7825	-2380.9421	-284.2484	-2386.19788852	-2385.2342
ts3'_b-aa-c2	-2381.5378	0.689507	-2380.7832	-2380.9407	-283.7738	-2386.19729742	-2385.2348

ts3'_b-aa-c3	-2381.5322	0.689198	-2380.7775	-2380.9	-283.7067	-2386.19552260	-2385.2316
ts3'_b-aa-c4	-2381.5355	0.689509	-2380.7807	-2380.94	-281.9868	-2386.19596982	-2385.2323
ts3'_b-aa-c5	-2381.5321	0.689292	-2380.7774	-2380.9369	-304.8330	-2386.19465426	-2385.2314
ts3'_b-aa-c6	-2381.5357	0.689362	-2380.7812	-2380.9	-269.5971	-2386.19504216	-2385.2323
ts3'_b-aa-c7	-2381.5313	0.689485	-2380.7765	-2380.9	-281.9394	-2386.19432240	-2385.23
ts3'_b-aa-c8	-2381.5352	0.689671	-2380.7803	-2380.9386	-303.3393	-2386.19238004	-2385.2307
ts3'_b-aa-c9	-2381.5315	0.689867	-2380.7766	-2380.9346	-298.0564	-2386.19151425	-2385.2285
ts3'_b-aa-c10	-2381.5398	0.689694	-2380.7852	-2380.9421	-273.9343	-2386.19221804	-2385.2285

ts3'_b-aa-c11	-2381.538	0.68989	-2380.7833	-2380.9395	-301.0522	-2386.18994428	-2385.2285
ts3'_b-aa-c12	-2381.5373	0.689751	-2380.7825	-2380.9397	-281.9361	-2386.19017998	-2385.2268

3. Ligand non-participation in C–H activation and insertion:

ts-1'a	-2146.1506	0.518113	-2145.5805	-2145.7119	-436.6324	-2150.25179663	-2149.412069
ts-1'b	-2374.8534	0.581988	-2374.211	-2374.3604	-1144.3739	-2379.42607373	-2378.5180592
ts-1'c1	-2374.8591	0.581302	-2374.2173	-2374.3664	-1121.5174	-2379.43433079	-2378.5270179
ts-1'c2	-2374.8622	0.581618	-2374.2202	-2374.3688	-1158.8650	-2379.43221037	-2378.5248558
ts-1'c3	-2374.8644	0.581842	-2374.2223	-2374.3706	-1167.8899	-2379.43111328	-2378.5238736
ts-1'c4	-2374.857	0.58183	-2374.2151	-2374.3631	-1158.6979	-2379.42807536	-2378.5198365

ts-1'c5	-2374.8399	0.581715	-2374.1982	2374.3455	-1119.7362	-2379.4117375 3	-2378.5042266

4. Arene site selectivity (*ortho*- vs *para*-):

ts-1o	-2010.3272	0.412335	-2009.8684	-2009.9894	-1136.4038	-2014.0809551 2	-2013.3227848
ts-1o-c2	-2010.3264	0.412728	-2009.8675	-2009.9873	-974.1986	-2014.0754951 4	-2013.3178916
ts-1o'	-2146.1916	0.518162	-2145.6217	-2145.7531	-1079.0146	-2150.2836752 5	-2149.445889
ts-3o	-2017.0025	0.520445	-2016.4309	-2016.5609	-330.9693	-2020.8357802 2	-2020.021731
int-4o	-2017.0373	0.523008	-2016.4633	-2016.5919	+	-2020.8678039 5	-2020.052957
ts-1p	-2010.3359	0.412169	-2009.8772	-2009.9984	-1147.9966	-2014.0921925 9	-2013.3325186
ts-1p-c2	-2010.3373	0.412306	-2009.8787	-2009.9992	-1129.4675	-2014.0909101 4	-2013.3321418

ts-1p'	-2146.1814	0.51829	-2145.6112	-2145.7425	-744.9454	-2150.27102572	-2149.431512
ts-3p	-2017.0115	0.52071313	-2016.4399	-2016.5688	-293.7	-2020.85068341	-2020.036795
int-4p	-2017.0464	0.522973	-2016.4725	-2016.6014	+	-2020.88460750	-2020.068617
5. Boltzmann sampling for 1,2-migratory insertion:							
***trans*-d1-c1**	-2017.0126	0.5201 25	-2016.4411	-2016.5715	-305.7022	-2020.85540249	-2020.038678
***trans*-d1-c2**	-2017.0142	0.5201 58	-2016.4428	-2016.5728	-293.1491	-2020.85566193	-2020.039368
***trans*-d1-c3**	-2017.0123	0.5198 17	-2016.4412	-2016.5716	-277.2951	-2020.85328579	-2020.0377419
***trans*-d1-c4**	-2017.0126	0.5200 1	-2016.4412	-2016.5718	-316.8	-2020.85300091	-2020.036383

***trans*-d1-c5**	-2017.0149	0.520454	-2016.4434	-2016.5728	-316.9	-2020.85392791	-2020.037906
***trans*-d1-c6**	-2017.0085	0.519782	-2016.4373	-2016.568	-317.3912	-2020.85229877	-2020.034701
***trans*-d1-c7**	-2017.0144	0.520509	-2016.4428	-2016.5725	-315.0322	-2020.85308536	-2020.037854
***trans*-d1-c8**	-2017.0168	0.520816	-2016.4453	-2016.5736	-311.5392	-2020.85368267	-2020.038209
***trans*-d1-c9**	-2017.0095	0.519896	-2016.4383	-2016.5685	-337.4155	-2020.84905704	-2020.033366
***trans*-d2-c1**	-2017.0141	0.519663	-2016.4431	-2016.5733	-282.5387	-2020.85718	-2020.040593
***trans*-d2-c2**	-2017.0149	0.519612	-2016.444	-2016.5737	-308.8734	-2020.856582	-2020.040347
***trans*-d2-c3**	-2017.0173	0.520244	-2016.446	-2016.575	-288.8986	-2020.85666626	-2020.040614

***trans*-d2-c4**	-2017.0178	0.520381	-2016.4465	-2016.575	-304.4657	-2020.855951	-2020.040502
***trans*-d2-c5**	-2017.0128	0.519858	-2016.4416	-2016.5714	-282.6224	-2020.8542	-2020.037271
***trans*-d2-c6**	-2017.0146	0.519844	-2016.4436	-2016.5729	-284.4537	-2020.854195	-2020.038113
***trans*-d2-c7**	-2017.0111	0.51986	-2016.44	-2016.5701	-262.2307	-2020.85319709	-2020.037409
***trans*-d2-c8**	-2017.0147	0.519773	-2016.4438	-2016.573	-303.2176	-2020.853935	-2020.038479
***trans*-d2-c9**	-2017.0105	0.520114	-2016.4393	-2016.5688	-258.7607	-2020.85091759	-2020.035064
***cis*-d1-c1**	-2017.0114	0.51977	-2016.4403	-2016.5706	-293.1446	-2020.85454809	-2020.038653
***cis*-d1-c2**	-2017.0143	0.520243	-2016.443	-2016.5723	-289.5588	-2020.85460815	-2020.038579

***cis*-d1-c3**	-2017.0094	0.51988	-2016.4381	-2016.5686	-305.4801	-2020.85298719	-2020.036652
***cis*-d1-c4**	-2017.0128	0.520244	-2016.4414	-2016.571	-296.5738	-2020.85400716	-2020.037311
***cis*-d1-c5**	-2017.0132	0.520084	-2016.4421	-2016.5713	-287.1232	-2020.85342783	-2020.038021
***cis*-d1-c6**	-2017.012	0.520164	-2016.4418	-2016.5688	-295.7306	-2020.85327945	-2020.037221
***cis*-d1-c7**	-2017.012	0.520787	-2016.4405	-2016.5689	-300.2449	-2020.84805177	-2020.033502
***cis*-d1-c8**	-2017.0103	0.520806	-2016.4386	-2016.5674	-308.1908	-2020.84782328	-2020.03263
***cis*-d1-c9**	-2017.0051	0.52114	-2016.4333	-2016.5618	-314.0032	-2020.84019556	-2020.025393
***cis*-d2-c1**	-2017.0103	0.520114	-2016.4389	-2016.5691	-298.4609	-2020.85288539	-2020.037075

***cis*-d2-c2**	-2017.0109	0.520454	-2016.4393	-2016.5691	-300.5416	-2020.85324996	-2020.03695
***cis*-d2-c3**	-2017.0124	0.520431	-2016.4411	-2016.5702	-287.7811	-2020.85360314	-2020.038019
***cis*-d2-c4**	-2017.0117	0.520184	-2016.4404	-2016.5702	-300.4347	-2020.85217076	-2020.037598
***cis*-d2-c5**	-2017.0101	0.520328	-2016.4386	-2016.5687	-309.4578	-2020.85155613	-2020.036441
***cis*-d2-c6**	-2017.0079	0.520258	-2016.4364	-2016.5667	-313.6194	-2020.85126903	-2020.034999
***cis*-d2-c7**	-2017.0082	0.520327	-2016.4368	-2016.5657	-296.732	-2020.84989422	-2020.033341
***cis*-d2-c8**	-2017.0036	0.520716	-2016.4319	-2016.5615	-311.8461	-2020.84614435	-2020.028735
***cis*-d2-c9**	-2017.0028	0.520698	-2016.4311	-2016.5606	-316.5124	-2020.84448830	-2020.028321

cy-d1-c1	-2015.8245	0.500939	-2015.2752	-2015.3997	-309.5106	-2019.64627570	-2018.840491
cy-d1-c2	-2015.8233	0.501342	-2015.2737	-2015.398	-314.2776	-2019.64579942	-2018.839852
cy-d1-c3	-2015.8266	0.501253	-2015.2771	-2015.4006	-301.2641	-2019.64457672	-2018.840282
cy-d1-c4	-2015.821	0.501307	-2015.2712	-2015.3956	-292.1391	-2019.64289929	-2018.83771
cy-d2-c1	-2015.8236	0.500956	-2015.2744	-2015.3978	-304.458	-2019.64570310	-2018.839656
cy-d2-c2	-2015.8252	0.50095	-2015.276	-2015.3993	-291.53	-2019.64481242	-2018.840874
cy-d2-c3	-2015.8193	0.500887	-2015.2698	-2015.3941	-276.5101	-2019.64393051	-2018.838106
cy-d2-c4	-2015.8225	0.501028	-2015.2733	-2015.3965	-303.1028	-2019.644799	-2018.83868655

6. Isodesmic studies:

pyridine	-247.76276	0.089473	-247.66596	-247.70411	+	-248.30904588	-248.2228936
ts-3-iso	-2264.7885	0.610871	-2264.1175	-2264.2672	**-325.2881**	-2269.16771081	-2268.26553
ts-3o-iso	-2264.8036	0.611869	-2264.1327	-2264.2776	**-285.3699**	-2269.16665412	-2268.26716
ts-3p-iso	-2264.7942	0.611633	-2264.123	-2264.2708	**-310.8723**	-2269.17001876	-2268.27014
7. *cis*-hexene product selectivity:							
***cis*-int-4**	-2017.0491	0.522286	-2016.4755	-2016.6050	+	-2020.89081831	-2020.074007
***cis*-ts-6**	-2017.0477	0.522116	-2016.4753	-2016.6026	**-56.3933**	-2020.88819118	-2020.071351
***cis*-int-7**	-2017.0458	0.521879	-2016.4733	-2016.6009	+	-2020.878591	-2020.062478
***cis*-ts-7**	-2017.04	0.517615	-2016.4721	-2016.5989	**-894.6881**	-2020.86995866	-2020.051674

***cis*-int-8**	-2017.0652	0.522118	-2016.4918	-2016.6211	+	-2020.88938870	-2020.07369804
***cis*-ts-6a**	-2017.0385	0.522431	-2016.4659	-2016.5931	**-99.8893**	-2020.87920898	-2020.061699
***cis*-int-7a**	-2017.0394	0.521802	-2016.467	-2016.5945	+	-2020.87708368	-2020.058029
***cis*-ts-7a**	-2017.0346	0.518017	-2016.4665	-2016.5928	**-978.8647**	-2020.86492859	-2020.046586
***cis*-int-8a**	-2017.0604	0.52288	-2016.4866	-2016.6149	+	-2020.88515958	-2020.069733
***cis*-ts-4b**	-2017.0163	0.520514	-2016.445	-2016.5739	**-82.2613**	-2020.86024466	-2020.041432
***cis*-int-5b**	-2017.0342	0.520372	-2016.4622	-2016.5930	+	-2020.87347141	-2020.056019
***cis*-ts-5b**	-2017.029	0.517817	-2016.4599	-2016.5898	**-366.9912**	-2020.86435208	-2020.049118

***cis*-int-6b**	-2017.0318	0.518939	-2016.4611	-2016.5918	+	-2020.86354955	-2020.05077
***cis*-ts-5b-c2**	-2017.0158	0.51803	-2016.4468	-2016.5756	**-480.8873**	-2020.85423166	-2020.038656
8. cyclohexene product selectivity:							
cy-int-4	-2015.8639	0.50327	-2015.3123	-2015.4358	+	-2019.68376601	-2018.876402
cy-ts-6a	-2015.8591	0.503392	-2015.3084	-2015.4297	**-88.5455**	-2019.67417990	-2018.868046
cy-int-7a	-2015.8591	0.502539	-2015.3084	-2015.4311	+	-2019.67414755	-2018.867609
cy-ts-7a	-2015.8477	0.498527	-2015.3017	-2015.4227	**-1032.9256**	-2019.65978358	-2018.851573
cy-int-8a	**-2015.8717**	**0.503244**	**-2015.3201**	**-2015.4435**	+	**-2019.67805522**	**-2018.872553**

2.9.11 Optimized geometries

Geometries of all optimized structures (in *.xyz* format with their associated energy in Hartrees) are included in a separate folder named *structures_xyz* with an associated README file. All these data have been deposited with this Supporting Information and uploaded to zenodo.org (DOI: 10.5281/zenodo.2775841).

3. References:

Full reference for ref (1):

Gaussian 16, Revision A.01, Frisch, M. J.; Trucks, G. W.; Schlegel, H. B.; Scuseria, G. E.; Robb, M. A.; Cheeseman, J. R.; Scalmani, G.; Barone, V.; Mennucci, B.; Petersson, G. A.; Nakatsuji, H.; Caricato, M.; Li, X.; Hratchian, H. P.; Izmaylov, A. F.; Bloino, J.; Zheng, G.; Sonnenberg, J. L.; Hada, M.; Ehara, M.; Toyota, K.; Fukuda, R.; Hasegawa, J.; Ishida, M.; Nakajima, T.; Honda, Y.; Kitao, O.; Nakai, H.; Vreven, T.; Montgomery Jr., J. A.; Peralta, J. E.; Ogliaro, F.; Bearpark, M.; Heyd, J. J.; Brothers, E.; Kudin, K. N.; Staroverov, V. N.; Kobayashi, R.; Normand, J.; Raghavachari, K.; Rendell, A.; Burant, J. C.; Iyengar, S. S.; Tomasi, J.; Cossi, M.; Rega, N.; Millam, J. M.; Klene, M.; Knox, J. E.; Cross, J. B.; Bakken, V.; Adamo, C.; Jaramillo, J.; Gomperts, R.; Stratmann, R. E.; Yazyev, O.; Austin, A. J.; Cammi, R.; Pomelli, C.; Ochterski, J. W.; Martin, R. L.; Morokuma, K.; Zakrzewski, V. G.; Voth, G. A.; Salvador, P.; Dannenberg, J. J.; Dapprich, S.; Daniels, A. D.; Farkas, Ö.; Foresman, J. B.; Ortiz, J. V; Cioslowski, J.; Fox, D. J. Gaussian, Inc., Wallingford CT, 2016.

(1) Frisch, M. J.; Trucks, G. W.; Schlegel, H. B.; Scuseria, G. E.; Robb, M. A.; Cheeseman, J. R.; Scalmani, G.; Barone, V.; Mennucci, B.; Petersson, G. A.; et al. Gaussian 16, Revision A.01. 2016.

(2) Yu, H. S.; He, X.; Li, S. L.; Truhlar, D. G. MN15: A Kohn–Sham Global-Hybrid Exchange–Correlation Density Functional with Broad Accuracy for Multi-Reference and Single-Reference Systems and Noncovalent Interactions. *Chem. Sci.* **2016**, *7* (8), 5032–5051.

(3) Andrae, D.; Häußermann, U.; Dolg, M.; Stoll, H.; Preuß, H. Energy-Adjustedab Initio Pseudopotentials for the Second and Third Row Transition Elements. *Theor. Chim. Acta* **1990**, *77* (2), 123–141.

(4) Weigend, F.; Ahlrichs, R. Balanced Basis Sets of Split Valence{,} Triple Zeta Valence and Quadruple Zeta Valence Quality for H to Rn: Design and Assessment of Accuracy. *Phys. Chem. Chem. Phys.* **2005**, *7* (18), 3297–3305.

(5) Weigend, F. Accurate Coulomb-Fitting Basis Sets for H to Rn. *Phys. Chem. Chem. Phys.* **2006**, *8* (9), 1057–1065.

(6) Mekareeya, A.; Walker, P. R.; Couce-Rios, A.; Campbell, C. D.; Steven, A.; Paton, R. S.; Anderson, E. A.; Ross Walker, P.; Couce-Rios, A.; Campbell, C. D.; et al. Mechanistic Insight into Palladium-Catalyzed Cycloisomerization: A Combined Experimental and Theoretical Study. *J. Am. Chem. Soc.* **2017**, *139* (29), 10104–10114.

(7) Deb, A.; Hazra, A.; Peng, Q.; Paton, R. S.; Maiti, D. Detailed Mechanistic Studies on Palladium-Catalyzed Selective C–H Olefination with Aliphatic Alkenes: A Significant Influence of Proton Shuttling. *J. Am. Chem. Soc.* **2017**, *139* (2), 763–775.

(8) Chai, J.-D.; Head-Gordon, M. Long-Range Corrected Hybrid Density Functionals with Damped Atom-Atom Dispersion Corrections. *Phys. Chem. Chem. Phys.* **2008**, *10* (44), 6615–6620.

(9) Marenich, A. V; Cramer, C. J.; Truhlar, D. G. Universal Solvation Model Based on Solute Electron Density and on a Continuum Model of the Solvent Defined by the Bulk Dielectric Constant and Atomic Surface Tensions. *J. Phys. Chem. B* **2009**, *113* (18), 6378–6396.

(10) Grimme, S. Supramolecular Binding Thermodynamics by Dispersion-Corrected Density Functional Theory. *Chem. – A Eur. J.* **2012**, *18* (32), 9955–9964.

(11) Funes-Ardoiz, I.; Paton, R. S. GoodVibes v1.0.1 http://doi.org/10.5281/zenodo.56091.

(12) E. D. Glendening, A. E. Reed, J. E. Carpenter, and F. W. NBO Version 3.1,.

(13) Contreras-García, J.; Johnson, E. R.; Keinan, S.; Chaudret, R.; Piquemal, J.-P.; Beratan,

D. N.; Yang, W. NCIPLOT: A Program for Plotting Noncovalent Interaction Regions. *J. Chem. Theory Comput.* **2011**, *7* (3), 625–632.

(14) Sosa, C.; Andzelm, J.; Elkin, B. C.; Wimmer, E.; Dobbs, K. D.; Dixon, D. A. A Local Density Functional Study of the Structure and Vibrational Frequencies of Molecular Transition-Metal Compounds. *J. Phys. Chem.* **1992**, *96* (16), 6630–6636.

(15) Godbout, N.; Salahub, D. R.; Andzelm, J.; Wimmer, E. Optimization of Gaussian-Type Basis Sets for Local Spin Density Functional Calculations. Part I. Boron through Neon, Optimization Technique and Validation. *Can. J. Chem.* **1992**, *70* (2), 560–571.

(16) Schrödinger, LLC. *The {PyMOL} Molecular Graphics Development Component, Version~1.8*; 2015.

(17) Maji, A.; Guin, S.; Feng, S.; Dahiya, A.; Singh, V. K.; Liu, P.; Maiti, D. Experimental and Computational Exploration of Para-Selective Silylation with a Hydrogen-Bonded Template. *Angew. Chemie - Int. Ed.* **2017**, *56* (47), 14903–14907.

(18) Maji, A.; Dahiya, A.; Lu, G.; Bhattacharya, T.; Brochetta, M.; Zanoni, G.; Liu, P.; Maiti, D. H-Bonded Reusable Template Assisted Para-Selective Ketonisation Using Soft Electrophilic Vinyl Ethers. *Nat. Commun.* **2018**, *9* (1).

(19) Wheeler, S. E.; Houk, K. N.; Schleyer, P. V. R.; Allen, W. D. A Hierarchy of Homodesmotic Reactions for Thermochemistry. *J. Am. Chem. Soc.* **2009**, *131* (7), 2547–2560.

(20) Wheeler, S. E. Homodesmotic Reactions for Thermochemistry. *Wiley Interdisciplinary Reviews: Computational Molecular Science*. 2012, pp 204–220.

(21) Peng, Q.; Duarte, F.; Paton, R. S. Computing Organic Stereoselectivity - from Concepts to Quantitative Calculations and Predictions. *Chem. Soc. Rev.* **2016**, *45* (22), 6093–6107.

(22) Fang, L.; Saint-Denis, T. G.; Taylor, B. L. H.; Ahlquist, S.; Hong, K.; Liu, S.; Han, L.; Houk, K. N.; Yu, J. Q. Experimental and Computational Development of a Conformationally Flexible Template for the Meta-C-H Functionalization of Benzoic Acids. *J. Am. Chem. Soc.* **2017**, *139* (31), 10702–10714.

4. Author Contributions

T.K.A. and R.M. conceived and developed the palladium catalyzed *meta*-selective C–H allylation. T.K.A. and R.M. optimized the reaction conditions. TKA, M.S.S., S.M. and N.P. prepared the starting materials and identified the substrates scope. TKA and M.S. conducted the mechanistic investigations. X.Z. designed and performed the computational studies. R.S.P supervised the computational studies. D.M. supervised the project. T.K.A. and X.Z. wrote the manuscript with input from R.S.P. and D.M. All authors read and commented on the manuscript.